The Astrophysical Journal Supplement Series, 140:389–406, 2002 June

CLASSIFICATION OF 2.4–45.2 MICRON SPECTRA FROM THE *INFRARED SPACE OBSERVATORY* SHORT WAVELENGTH SPECTROMETER[1]

Kathleen E. Kraemer,[2,3] G. C. Sloan,[4,5] Stephan D. Price,[2] and Helen J. Walker[6]

Received 2001 September 4; accepted 2002 January 18

ABSTRACT

The *Infrared Space Observatory* observed over 900 objects with the Short Wavelength Spectrometer in full-grating scan mode (2.4–45.2 μm). We have developed a comprehensive system of spectral classification using these data. Sources are assigned to groups based on the overall shape of the spectral energy distribution (SED). The groups include naked stars, dusty stars, warm dust shells, cool dust shells, very red sources, and sources with emission lines but no detected continuum. These groups are further divided into subgroups based on spectral features that shape the SED such as silicate or carbon-rich dust emission, silicate absorption, ice absorption, and fine-structure or recombination lines. Caveats regarding the data and data reduction, as well as biases intrinsic to the database, are discussed. We also examine how the subgroups relate to the evolution of sources to and from the main sequence and how this classification scheme relates to previous systems.

Subject headings: catalogs — infrared: ISM — infrared: stars — ISM: general — ISM: lines and bands — stars: fundamental parameters

On-line material: machine-readable table

1. INTRODUCTION

Spectral classification organizes astronomical sources into groups with similar properties based on the general or detailed morphology of their spectral energy distributions (SEDs). Consequently, the classification criteria depend on the wavelength region and spectral resolution used. Both of these parameters must be uniform in order to create consistent criteria for arranging the sources in a database. The similarities and differences that result from applying a successful classification system to a sufficiently large sample of sources not only improve our knowledge about the sources but provide a basis for understanding the physical parameters of the objects.

The best example of how a classification system can lead to insight into the physical properties of the objects studied is provided by optical spectral classification (e.g., Hearnshaw 1986). From the earliest systems based on general color (e.g., Rutherford 1863), several competing systems emerged based on spectral line ratios (e.g., Secchi 1866, 1868; Vogel 1874; Vogel & Wilsing 1899; Pickering 1890). Of these, the Harvard system used originally in the Draper Memorial Catalogue (Pickering 1890) grew to predominate as a result of the large number of sources classified (>10,000) and served as the basis for the Henry Draper Catalogue (beginning with Cannon & Pickering 1918).

The MK spectral classification system evolved from the Harvard system (e.g., Morgan 1938; Morgan, Keenan, & Kellman 1943). This two-dimensional system provided the clues necessary to disentangle the different stages of the life cycle of a star and the relation of intrinsic parameters such as mass and metallicity to directly observable properties. MK spectral classification remains the single most powerful diagnostic tool available to astronomers when applied to naked stars, i.e., stars not embedded in dust.

Unfortunately, the very early and very late stages of stellar evolution rarely involve naked stars. The sources are deeply embedded within interstellar dust clouds or circumstellar dust shells, either of which absorb the optical radiation and reemit it in the infrared. This dust can absorb so much of the optical radiation from the star that traditional classification based on the photospheric properties of the star in the optical is difficult, if not impossible. Near-infrared observations can often penetrate the obscuring dust, permitting direct measurements of the stellar photosphere. The spectral region between 1 and 9 μm is rich in atomic and molecular lines that trace temperature and luminosity. For example, CO, SiO, and water vapor are sensitive indicators in oxygen-rich stars, even with low spectral resolution; the Phillips and Ballick-Ramsey C_2 bands as well as CN and CO serve for carbon stars. However, the emission from the dust distorts the photospheric continuum and fills in the absorption features, making analysis difficult. Observations in the thermal infrared trace the emission from the dust itself. The characteristic SED of the dust is distinctive enough to serve as the basis for classification (Little-Marenin & Price 1986; Little-Marenin et al. 1987; Cheeseman et al. 1989).

[1] Based on observations with the *Infrared Space Observatory* (*ISO*), a European Space Agency (ESA) project with instruments funded by ESA Member States (especially the Principle Investigator countries: France, Germany, Netherlands, and United Kingdom) and with the participation of the Institute of Space and Astronautical Science and the National Aeronautics and Space Administration (NASA).

[2] Air Force Research Laboratory, Space Vehicles Directorate, 29 Randolph Road, Hanscom AFB, MA 01731; kathleen.kraemer@hanscom.af.mil, steve.price@hanscom.af.mil.

[3] Institute for Astrophysical Research, Boston University, Boston, MA 02215.

[4] Institute for Scientific Research, Boston College, Chestnut Hill, MA 02467; sloan@ssa1.arc.nasa.gov.

[5] Infrared Spectrograph Science Center, Cornell University, Ithaca, NY 14853-6801.

[6] Rutherford Appleton Laboratory, Chilton, Didcot, Oxon, OX11 0QX, UK; H.J.Walker@rl.ac.uk.

The infrared spectra obtained by the Low-Resolution Spectrometer (LRS) on the *Infrared Astronomical Satellite* (*IRAS*) are the best example of a nearly complete, self-consistent database that is ideal for spectral classification. These spectra cover wavelengths from 7.7 to 22.7 μm at a spectral resolution of $\lambda/\Delta\lambda \sim 20$–60. The original LRS atlas contained spectra from 5425 sources (*IRAS* Science Team 1986). Volk et al. (1991) expanded the database to 6267, and Kwok, Volk, & Bidelman (1997) extracted almost 5000 additional spectra from the raw data, to create a spectral database of 11,224 sources, making the LRS observations the largest infrared spectral database to date. This database includes most of the 12 μm objects in the sky brighter than 10 Jy at 12 μm (1 mag), and several infrared classification systems have been developed from it.

The initial LRS classification scheme (*IRAS* Science Team 1986; *IRAS* Explanatory Supplement 1988) sorted the original database of 5425 sources into 10 groups, essentially based on the dominant spectral feature in the 10 μm region. These groups were subdivided further, usually by the strength of the dominant feature. The AutoClass algorithm (also known as AI for artificial intelligence) used a Bayesian algorithm to sort the database into self-consistent classes with no a priori input about the nature of the spectra (Cheeseman et al. 1989; Goebel et al. 1989). Kwok et al. (1997) used one-letter codes to identify the character of each spectrum in the expanded database (11,224 sources). These various classification systems have divided the LRS database into distinct sets of spectral classes. However, none of these systems have been applied to a substantial number of spectra from instruments other than the LRS.

Other schemes focused on subsets of the LRS database. For example, Little-Marenin & Little (1988, 1990, hereafter collectively LML) classified evolved oxygen-rich stars based on their dust emission characteristics. This system, as modified by Sloan & Price (1995, 1998, hereafter collectively SP), has also been applied to ground-based spectral measurements (e.g., Creech-Eakman et al. 1997; Monnier, Geballe, & Danchi 1998).

Spectra taken by the Short Wavelength Spectrometer (SWS) on the *Infrared Space Observatory* (*ISO*; Kessler et al. 1996; de Graauw et al. 1996) are now publicly available. In this paper we focus on the full-range, moderate-resolution spectra obtained in the SWS01 observing mode. These observations are over a greater wavelength range than the LRS database (2.4–45.2 μm compared to 7.7–22.7 μm) and at a higher spectral resolution (>300–400 vs. 20–60). The SWS01 spectral resolution is sufficient for detailed examination of band structure and atomic fine-structure lines. The extended wavelength range includes both the near-infrared spectral region, which is dominated by molecular bands from stellar photospheres, and the thermal infrared region, which is dominated by dust emission. The LRS database is compromised by inadequate wavelength coverage on the short-wavelength side of the strong spectral features produced by silicate dust (10 μm) and silicon-carbide grains (11.5 μm), making it difficult to unambiguously define the stellar continuum.

ISO obtained observatory-style pointed observations, whereas *IRAS* obtained spectra as an adjunct to the main survey with the LRS as a secondary instrument. Consequently, the SWS database only contains full-range spectra of ~910 specifically targeted sources (1248 total spectra, including duplicates and off positions). To ensure that *ISO* obtained SWS spectra of as wide a variety of sources as possible, the observing lists of the STARTYPE proposals[7] targeted sources in categories that were underrepresented in the infrared classification systems (§ 2.1). The result is a robust database of infrared spectra that is the basis for our infrared spectral classification system.

We describe the sample of the observed sources and the structure and calibration of the spectral data in § 2. Section 3 details the criteria for the classification system, which we discuss in § 4. The actual classifications are presented in Appendix A.

2. OBSERVATIONS AND DATA ANALYSIS

2.1. *The Sample*

2.1.1. *Source Selection*

The SWS database contains observations obtained for a wide range of individual observing projects. A series of observing proposals, referred to collectively as the STARTYPE proposals, was developed to supplement observations from other dedicated- and open-time experiments. The original observing lists included at least one source from each category defined by the MK spectral types, LRS classifications, AutoClass classifications, and the spectral templates in the Galactic Point-Source Model (Wainscoat et al. 1992). While the MK classification system is familiar to most readers, the infrared classification systems may be less so. Therefore, we describe below the three infrared classification systems used to create the STARTYPE observation lists.

The LRS classifications presented in the LRS atlas (*IRAS* Science Team 1986) used a two-digit scheme to describe a spectrum. The scheme subjectively divided the spectra into 10 groups (identified by the first digit) based on spectral morphology and, in part, on ideas about the underlying physics producing the spectra. For blue sources (i.e., flux decreasing with wavelength), the first digit represents (1) featureless spectra, (2) silicate emission, (3) silicate absorption, or (4) carbon-rich dust emission features. Red sources were assigned a first digit of 5, 6, or 7 (analogs of 1, 2, or 3). Spectra dominated by emission lines were divided into (8) those with unidentified infrared (UIR) bands and (9) those without UIR bands. Miscellaneous spectra were assigned an initial digit of 0. The second digit was typically based on the strength of the features identified by the first digit. In general, the spectral morphology is clearly different among the groups, but some inconsistencies and misclassifications exist.

The AutoClass scheme (Goebel et al. 1989; Cheeseman et al. 1989) used AI to sort the LRS spectra into a series of self-consistent classes. By separating features on the basis of both shape and strength, this method distinguished subtleties not addressed by the LRS atlas characterizations, which separated features based on strength alone. It also found weak features that had been previously undetected.

Selecting sources only from classification systems based on the LRS database excludes information about the wavelength regions not covered by the LRS, that is, shortward of 7.7 μm and longer than 22 μm. To address this shortcoming,

[7] The STARTYPE proposals received *ISO* project names STARTYP1, STARTYP2, and ZZSTARTY.

TABLE 1
IRAS POPULATION COVERAGE

CLASS	SUBCLASS									
	0	1	2	3	4	5	6	7	8	9
LRS Atlas Classifications										
0	0, 1/1	6, 21/313	3, 3/4	0, 1/1	1, 5/12	8, 6/32	...	...	...	...
1	1, 1/2	0, 1/1	2, 4/20	3, 15/116	7, 34/324	19, 22/480	22, 20/390	11, 16/349	40, 21/460	7, 4/96
2	...	9, 10/43	16, 23/151	9, 13/137	10, 16/155	5, 14/163	9, 17/175	8, 14/197	8, 14/210	12, 27/499
3	...	9, 10/46	5, 11/49	1, 4/30	0, 6/22	2, 4/19	0, 3/9	1, 1/8	4, 3/8	6, 4/39
4	...	6, 6/26	15, 16/152	6, 13/133	9, 10/113	5, 6/64	1, 2/21	1, 2/15	0, 1/3	1, 2/11
5	6, 11/51	2, 3/4	0, 2/4	1, 4/4	...	...	...	...	...	...
6	...	...	2, 1/2	0, 0/3	1, 1/6	0, 0/3	1, 1/4	1, 1/7	0, 0/3	9, 16/50
7	...	1, 4/7	4, 4/9	3, 2/9	3, 2/7	2, 1/8	3, 2/5	1, 0/3	0, 0/1	4, 4/18
8	9, 18/42	12, 9/23	3, 2/3	...	...	1, 1/1	...	...	...	...
9	...	9, 12/24	3, 3/5	...	3, 2/6	6, 7/13	1, 1/1	...	...	...
AutoClass Classifications										
α	14, 18/155	0, 2/39	1, 2/23	0, 0/27	2, 4/60	4, 10/91	1, 5/83			
β 0–9	11, 23/224	10, 17/171	3, 8/144	0, 1/51	0, 5/102	0, 1/36	1, 1/40	1, 1/58	12, 14/172	0, 3/89
β 10–13	0, 0/31	9, 10/126	0, 0/7	0, 0/12	...	...	...	...	...	...
γ	42, 49/102	23, 22/55	...	...	...	...	...	...	...	...
δ	44, 27/256	14, 7/236	2, 10/65	0, 2/78	0, 5/42	2, 2/130	0, 2/80	0, 3/48	6, 7/137	
ϵ	6, 2/16	6, 20/138	5, 7/83	0, 1/3	...	...	...	...	...	...
ζ	17, 38/98	1, 3/45	4, 4/28	17, 16/63	19, 25/121	...	...	...	...	...
η	0, 9/62	2, 3/43	...	...	...	...	...	...	...	...
θ	0, 4/15	...	...	...	...	...	...	...	...	...
λ 0–9	0, 0/1	0, 1/22	0, 0/5	0, 0/3	0, 0/3	...	1, 1/45	6, 5/124	...	0, 0/1
λ 10–19	0, 1/32	0, 1/26	4, 9/58	0, 0/1	0, 0/1	0, 0/1	1, 1/30	0, 0/7	1, 2/77	1, 0/4
λ 20–29	11, 23/121	1, 7/107	0, 1/5	...	0, 8/120	12, 18/179	0, 0/5	2, 3/81	10, 8/103	0, 1/11
λ 30–35	33, 36/273	0, 1/37	0, 0/4	0, 0/5	16, 23/139	0, 0/5	...	...	...	...

NOTE.—In each class, the numbers given as a, b/c are (a) the number of sources actually observed, (b) the number selected for observation by STARTYPE, and (c) the total number in the subclass.

the STARTYPE experiments also selected sources based on the spectral templates in the Galactic Point-Source Model (Wainscoat et al. 1992). Sources in this scheme are divided into classes based on either the MK spectral classifications or location in the [12]−[25], [25]−[60] color plane. Cohen et al. (1990) grouped sources in the [12]−[25], [25]−[60] plane and created prototypical spectral templates used in the Wainscoat et al. (1992) Galactic Point-Source Model.

An initial list of 1316 sources brighter than 40 Jy at 12 μm was compiled by randomly selecting $\sim$10% of the sources that were used to create the classification schemes described above. Because all three infrared schemes use the LRS spectra, roughly 25% of the sources were randomly selected from the LRS atlas and then sorted by LRS class. When a particular LRS subclass was well populated after the initial selection, sources associated with objects in other catalogs were preferentially chosen as a result of the additional information available on them. Because the 12 μm flux criterion discriminated against red and emission-line objects, the flux limit was lowered to 5 Jy at 12 μm to include 347 red objects (LRS classes 5*n*–9*n*) and to increase the number of sources in other underpopulated LRS classes. The resulting list was tabulated in terms of the number of sources in each LRS and AutoClass subclass. If a subclass had more than 10 objects in the list, objects with higher quality LRS spectra were preferentially selected. Noisy counterparts of other, better defined subclasses and faint, unique classes (such as 01 or θ0) were proportionately underrepresented in the observing list. The final 10% observing list comprised somewhat less than 800 sources.

Given the time constraints of the *ISO* mission, only a fraction, approximately 1/10, of the 10% list could be observed. The initial STARTYPE observing list sparsely, but uniformly, sampled the LRS and AutoClass subclasses (Table 1) and populated the MK classes. Because astrophysically interesting sources included in our list would likely be observed by other experimenters, we deferred the majority of our observations until we had surveyed the observing lists for the dedicated- and open-time SWS01 spectra to determine which spectral classes were underrepresented. As expected, the SWS01 observing lists of other experimenters sampled the red LRS classes (5*n*–9*n*) and the equivalent AI classes well. The other classes were not as well sampled. We then concentrated the STARTYPE observations on the types of objects not observed by other *ISO* investigators, such as those with featureless continua and carbon stars with small circumstellar excesses. Therefore, additional sources within LRS classes 1*n*, 2*n*, and 4*n* were included in the STARTYPE observing list to provide more spectral representatives, particularly for the important subclasses 29, 43, and 44. Several LRS class 3*n* sources were also included to correct the slight underrepresentation across the entire class. In this sample, stars of MK luminosity class V are well represented from B to early G, IIIs from early G to late M, and there is a sprinkling of temperature classes for the Is and IIs. Because M dwarfs are faint, we used the PHT spectrometer PHT-S to obtain spectra of six

sources in the M dwarf sequence (S. D. Price et al. 2002, in preparation).

The observing scheme worked well. Of the ~910 individual sources with SWS01 spectra, 275 were among the 800 sources in our 10% list. This number increased to 379 if we had chosen to populate our subclasses to the 10% limit with the sources actually observed, although the coverage is not as uniform (see below). Table 1 shows how the number of sources observed compares to the number proposed and to the total number of objects in each LRS and AutoClass subclass.

2.1.2. *Selection Effects*

Although the STARTYPE program aimed at producing a uniform sample, other programs did not. Objects in most programs were chosen with a particular research objective in mind, to investigate a particular phenomenon or a specific source. Sources with unusual features, intrinsically more interesting than sources that are more typical, were observed more often than they would have been in a completely uniform sample. For example, η Carina, as a unique object, would likely not have been observed in a randomly selected sample of the 1248 objects but was observed twice with SWS. However, the tendency to observe more unusual sources makes it more likely that the grid of subgroups for classification includes most of the possible types of infrared spectra.

Comparing the number of objects in each LRS and AI class with the number actually observed (Table 1) provides some insight into the bias of the SWS database. Although 47% of the STARTYPE 10% list was observed, the coverage of the *IRAS* classes (either LRS or AI) was significantly less uniform than the STARTYPE selections. For example, STARTYPE proposed to observe 34 of the 324 objects (10%) in LRS class 14, but the SWS database includes only seven (2%). This apparently uninteresting group consists of nominally naked stars with spectral indices of $\beta \sim 2$ (*IRAS* Explanatory Supplement 1988); in reality, these sources exhibit low-contrast dust emission (see LML and SP). In contrast, a group of truly naked stars with high signal-to-noise ratio defined by AutoClass $\delta 0$ (Cheeseman et al. 1989; Goebel et al. 1989) had 44 of 256 objects (16%) observed instead of the 27 suggested by STARTYPE, primarily because this group included the chosen calibration stars. Roughly 15% of the LRS and AutoClass classes had significantly fewer sources observed than if the STARTYPE sample had been followed, including several that in the end had no members observed. On the other hand, the SWS database includes more than twice as many planetary nebulae (PNs) and star-forming regions—source types that include the brightest objects in the infrared sky—as the LRS atlas (*IRAS* Science Team 1986), significantly expanding the available database on these important object types.

2.2. *Data from the ISO Data Archive*

The SWS obtained 1248 SWS01 spectra of over 900 different sources. The SWS01 spectra[8] cover wavelengths from 2.4 to 45.2 μm in 12 spectral segments (or bands). The bands vary in length from 0.2 (band 1A: 2.4–2.6 μm) to over 16 μm (band 4: 29–45 μm). Each includes data from 12 individual detectors taken in two scan directions ("up" and "down" scans), giving a total of 24 discrete spectra in each spectral segment. Thus, to produce one full-scan spectrum from the SWS, 288 individual spectra must be calibrated and combined.

The standard "basic science" format for SWS spectra from the *ISO* Data Archive (IDA) is the Auto-Analysis Result (AAR) produced by the Off-Line Processing (OLP) pipeline. To classify the spectra, we typically used the browse product, which was created from OLP Version 7.1. The browse product collapses the individual spectral scans to one usable spectrum, which usually sufficed for classification. For problematic spectra, we used a preliminary release of OLP Version 10.0, combining the data into one spectrum using software written at the Air Force Research Laboratory. Sloan et al. (2001a) will present further details of this method, as well as a spectral atlas of the 1248 spectra.

Despite efforts to calibrate the flux of each spectral segment in the standard pipeline, discontinuities often exist at the boundaries between each of the 12 bands (Sloan, Kraemer, & Price 2001b; Kraemer, Sloan, & Price 2001; Shipman et al. 2001). For compact sources (smaller than the aperture), this problem most likely results from errors in satellite pointing (Shipman et al. 2001). Since the point-spread function (PSF) is comparable to the angular size of the aperture, a slight offset from the center of the aperture will truncate the PSF.

A formal solution to the discontinuities does not yet exist, but a work-around has produced satisfactory results. Although the bands have sharply defined edges, adjacent bands include overlap regions of ~0.15–2.0 μm. While only data from one band were considered to be "in-band" for a particular overlap region, with a well-calibrated relative spectral response function (RSRF), the "out-of-band" data can often be used to verify spectral features, the shape of the SED in that overlap region, and, most importantly, the flux level. To correct for the band-to-band discontinuities, the flux from a (usually) well-behaved spectral segment was chosen to be the fiducial segment and the other segments normalized to it, usually by a multiplicative factor. An additive factor was used for fainter sources where dark current variations might dominate gain variations. The same band could not be used for all sources as a result of the lack of flux in that band for certain SEDs. Band 1B (2.60–3.02 μm) served as the fiducial segment for sources dominated by flux from the stellar photosphere. For red sources peaking beyond ~15 μm, band 3C (16.5–19.5 μm) was the fiducial segment.

The detectors of bands 2 (4.08–12.0 μm, Si:Ga) and 4 (29.0–45.2 μm, Ge:Be) exhibit memory effects that can lead to differences in signal between the up and down scans (e.g., Sloan et al. 2001b; Kraemer et al. 2001). This problem manifests itself as a variation in dark current during a scan, the magnitude of which depends on the recent flux history of the detector. The SWS Interactive Analysis[9] (IA) routine *dynadark* was developed to model the dark current in band 2. The algorithm in this routine is based on the Fouks-

[8] Hereafter, the set of 1248 SWS01 spectra is referred to as "the SWS database."

[9] The SWS Interactive Analysis system is developed and maintained by the SWS consortium members (Space Research Organization of the Netherlands, Max-Planck-Institut für Extraterrestrische Physik, Katholiede Universiteit Leuven, and the European Space Agency).

Schubert formalism (Fouks & Schubert 1995; Fouks 2001; Kester, Fouks, & Lahuis 2001), which accounts for nonlinear responses in the flux history of the detectors. In its current form, this routine behaves erratically. It can substantially improve the band 2 data, but it can also overcorrect the data, degrading the match between up and down segments in band 2A or 2B (Sloan et al. 2001b; Kraemer et al. 2001). The pipeline 10 processing automatically includes the *dynadark* routine.

The memory effect in band 4 affects the shape of the spectrum longward of $\lambda \sim 38$–40 μm. The degree to which a spectrum is affected depends on the underlying SED of the source and its brightness, as well as when during the mission and at what speed the observation was made. Changes in the calibration strategy involving photometric checks and dark current measurements by revolution 200 helped to some extent. However, the underlying problem with the memory effects remains unsolved.

Discontinuities in the 26–30 μm region are caused by a combination of changing aperture size (especially for extended sources), pointing issues, a light leak in band 3D, and the poor behavior of band 3E in many spectra. The first two problems require multiplicative corrections (to first order). The light leak appears at the long-wavelength end of band 3D and results from radiation from band 3A leaking through the filter for band 3D. When it occurs, it invalidates data in band 3D beyond $\sim$27.3 μm. Band 3E often contains very noisy data, especially at fainter flux levels. While the boundary between bands 3D and 3E is officially 27.5 μm (Leech et al. 2001), the former cannot be used beyond 27.3 μm as a result of the light leak, and the latter is invalid below 27.7 μm. As a result, normalization of one band to the other requires extrapolation of the data in the gap between them. Fortunately, band 4 provides relatively reliable data at wavelengths down to 27.7 μm in OLP 10.0, even though its official cutoff is 29.0 μm. This extension allows normalization of band 4 directly to band 3D by extrapolation, bypassing the unreliable data in band 3E.

The procedure used to reduce the band discontinuities assumes that the flux levels for band 1B or 3C are reliable. Any errors in the absolute flux level within those bands will be propagated to the other bands through the normalization process. Furthermore, if the wrong reference band is chosen or an overlap region is unusually noisy, incorrect normalization can degrade the data. This problem is especially acute for weak sources with peak fluxes less than $\sim$25 Jy. The impact of these calibration issues on the classification effort is discussed in § 4.1.

2.3. *Classification Method*

We created a list of all SWS01 observations, regardless of object type or quality flag, from the IDA, giving a total of 1248 spectra. The browse product spectrum for each of the 1248 observations was examined for quality. If a spectrum had no apparent signal, it was set aside; this included most observations designated as off or reference positions by the observer. (If a spectrum had a discernible signal, it remained in the sample regardless of designation, such as the observation originally designated M17NOFF.) Roughly 35 objects contained no signal because the observer entered incorrect coordinates. The OLP software flagged an additional 30 or so spectra as having instrumentation, telemetry, pointing, or quality problems, but we classified them anyway.

Two of the authors (K. E. K. and G. C. S.) classified the sources independently, without prior knowledge of the MK spectral type, LRS class, or AutoClass category. The separate classifications were then compared and combined into a single scheme. Sources for which the placement was uncertain or unclear were reprocessed and reexamined. Typically this reprocessing resolved the ambiguity, although often the assigned classification included a single or double colon to indicate uncertainty (see below).

3. THE CLASSIFICATIONS

We established three levels of classification.[10] The level 1 categories (hereafter "groups") are sorted based on the general morphology of the SED, which is determined primarily by the temperature of the strongest emitter (be it stellar or dust). Level 2 classification places each spectrum into a self-consistent subgroup based on the presence of prominent spectral features, such as silicate dust emission or absorption, carbon-rich dust emission, or atomic fine-structure lines.[11]

Level 3 classification will be the arrangement of spectra within a given subgroup into a sequence. This is a complex, interactive project left for the future. Some studies have reached level 3 classification for certain subgroups already well defined by previous spectral databases. For example, SP have already developed a sequence for oxygen-rich dust spectra produced by optically thin circumstellar shells.

3.1. *Level 1 Classification*

The level 1 classes primarily depend on the temperature of the dominant emitter. Five main categories emerged, ranging from the hottest objects such as naked stars (1) to the coolest objects such as protostellar cores (5). Additional categories include spectra with emission lines but no detected continuum (6) and spectra that either contain no classifiable flux or are flawed for some other reason (7). These seven categories are defined as follows:

1. Naked stars. Photospheric emission with no apparent influence from circumstellar dust dominates these spectra. All sources have optical identifications with known and well-classified stars.
2. Stars with dust. The SEDs are primarily photospheric at shorter wavelengths, but they also show noticeable or significant dust emission at longer wavelengths. Most sources are red supergiants or are associated with the asymptotic giant branch (AGB).
3. Warm, dusty objects. These sources are dominated by emission from warm dust. Any photospheric contribution from an embedded star is either absent or significantly less than the peak emission. The emission typically peaks between $\sim$5 and $\sim$20 μm, which implies dust temperatures hotter than $\sim$150 K. The majority of these spectra arise from deeply enshrouded AGB sources, transition objects, PNs, or other evolved sources.

[10] Use of existing LRS classifications was considered. However, those classes were based on a limited spectral range and focused too strongly on the strength of a single feature. This scheme was rejected as inadequate to describe the full range of SWS spectra (see § 4.2.2).

[11] Acceding to a request by the editor to name our classification scheme, we hereby christen it "the KSPW system."

4. Cool, dusty objects. These objects are dominated by cooler dust emission, the peak of which occurs within the SWS spectral range but longward of ~20 μm. Most sources in this group are PNs, AGB stars, and transition objects, although many are young stellar objects (YSOs).

5. Very red objects. These objects have rising spectra toward longer wavelengths through at least the end of band 4. Most sources are star-forming regions or PNs.

6. Continuum-free objects but with emission lines. These sources do not have enough continuum emission to allow an unambiguous placement in another group. Emission lines, typically atomic fine-structure lines, dominate the spectra. Objects in this group include supernova remnants and novae. Because these spectra are often difficult to discern from the class 7 spectra, this group may not contain all possible members observed by *ISO*.

7. Flux-free and/or fatally flawed spectra. This group includes objects with no detected flux or flux levels insufficient for classification. In addition to intrinsically faint objects, this group contains observations with incorrect coordinates, observations intentionally offset from sources (off positions), and flagged observations. Spectra with enough flux to allow classification appear in the appropriate group whenever possible despite flags or off-target coordinates.

3.2. *Level 2 Classification*

Level 2 classification separates the level 1 groups into subgroups based on the spectral features superimposed on the overall SED. Each subgroup has a one-, two-, or three-letter designation that succinctly indicates the type of dust and most prominent feature(s), as described below and summarized in Table 2. In addition to the letter designations, one-character suffixes describe any unusual properties of the spectrum (Table 3).

The initial letter of the designation indicates the overall "family" to which an object belongs. The three most important families are "S," "C," and "P." "S" indicates oxygen-rich dust material such as silicate or alumina grains, whereas "C" indicates carbon-rich material. "P" indicates PNs, which typically have spectra rich in emission lines.

TABLE 2
Level 2 Classification Definitions

Class	Description
SE	Silicate (or oxygen-rich) dust emission (10–12 and 18–20 μm)
SB	Silicate emission in self-absorption (10 μm)
SA	Silicate absorption (10–12 μm)
SC	Silicate emission from crystalline grains (33, 40, 43 μm)
SEC	Silicate emission from crystalline grains (11, 19, 23, 33 μm)
CE	Carbon-rich dust emission, primarily from SiC (11.5 μm)
CR	Carbon-rich dust emission in a reddened shell (with features at 11.5 and 26 μm, often 13.7 μm absorption)
CT	8, 11.5, 21, 26 μm, no 13.7 absorption
CN	Carbon-rich nebulae
C/SE	Carbon-rich, plus silicate emission (10–12 μm)
C/SC	Carbon-rich, plus crystalline silicate emission
U/SC	Crystalline silicate and UIR emission features
U	Prominent UIR emission features
PN	Many prominent atomic fine-structure lines typical of PNs
PU	As PN, but with strong UIR emission
W	Emission peaks 6–8 μm
F	Basically featureless
E	Strong emission lines
M	Miscellaneous

TABLE 3
Level 2 Suffixes

Suffix	Description
e	Emission lines (e.g., H recombination, atomic fine structure)
u	UIR features present, but not dominant feature
p	Fits in given category but is peculiar
:, ::	Uncertain (either noisy or odd)

The second and third letters, if used, indicate the presence of one or more specific spectral features. The letter combinations present in groups 2–5 are as follows:

SE: silicate or oxygen-rich dust emission feature at ~10–12 μm, usually accompanied by a secondary emission feature ~18–20 μm.

SB: self-absorbed silicate emission feature at 10 μm, usually showing emission peaks at 9 and 11 μm. The secondary emission feature ~18–20 μm is common.

SA: silicate absorption feature at 10 μm. The 18–20 μm feature can be in emission or absorption. Features from crystalline silicate emission may also be present at longer wavelengths.

SC: crystalline silicate emission features, especially at ~33, 40, and/or 43 μm. No significant silicate features are apparent at ~10 μm.

SEC: crystalline silicate emission features, especially at 11 μm, usually at ~19, 23, and 33 μm, and often at 40 and/or 43 μm. The presence of crystalline silicates has shifted the emission feature at 10 μm as a result of amorphous silicate grains ~1 μm to the red. The presence of other crystalline features distinguishes this feature from the self-absorbed silicate emission (SB) feature, which also peaks at ~11 μm.

CE: carbon-rich dust emission dominated by the silicon carbide emission feature at ~11.5 μm. The shape and wavelength of this feature differ substantially from the SB and SEC features at 11 μm, and any uncertain cases can be resolved by the presence of a narrow absorption feature at 13.7 μm (due to C_2H_2; e.g., Aoki, Tsuji, & Ohnaka 1999; Cernicharo et al. 1999; Volk, Xiong, & Kwok 2000).

CR: carbon-rich dust emission showing a reddened continuum (due to a strong contribution from amorphous carbon), the SiC emission feature at ~11.5 μm, and another emission feature at ~26–30 μm.

CT: carbon-rich dust emission characterized by a red continuum and emission features at 8, 11.5, 21, and 26–30 μm. The "T" stands for the 21 μm emission feature, which is the primary discriminant between CR and CT.

CN: carbon-rich proto–planetary nebulae (PPNs) with 11.5 μm emission or the 13.7 μm absorption features and much redder SEDs as compared to the CRs.

C/SC: carbon-rich features in the blue half of the spectrum, combined with crystalline silicate emission features at 33, 40, and/or 43 μm.

C/SE: carbon-rich features in the photospheric emission, combined with silicate or oxygen-rich dust emission at ~10–12 μm. These are the silicate carbon stars (e.g., Little-Marenin 1986; Lloyd Evans 1990).

TABLE 4
LEVEL 1–2 CROSS-REFERENCES AND STATISTICS

	LEVEL 1						
LEVEL 2	Group 1	Group 2	Group 3	Group 4	Group 5	Group 6	Group 7
N	49/59						
NO	49/90						
NC	4/7						
SE		a: 59/72[a] b: 26/43 c: 42/53	21/27	25/27	7/7		
SB		...	9/12	7/8	...		
SA		...	2/3	25/30	50/63		
SC		...	...	14/19	...		
SEC		...	...	10/13	...		
CE		29/53	6/6	...	...		
CR		...	9/9	12/14	...		
CT		...	...	9/12	...		
CN		...	...	5/5	...		
C/SE		3/3	...	...	...		
C/SC		...	...	1/2	...		
U/SC		...	...	9/14	...		
U		2/3	...	...	19/26		
PN		...	...	24/35	6/6		
PU		...	...	11/16	...		
W		...	13/15	...	...		
UE		...	...	...	89/96		
E	7/9	3/4	...	...	18/18		
F		...	...	15/16	18/19		
M	11/13	6/6	...	4/8	10/10		
Total	120/178	170/237	60/72	171/219	217/245	100/113	82+/184

NOTE.—The format of the entries is sources/spectra. "Spectra" refers to the total number of observations in a particular category. "Sources" refers to the number of spatially distinct objects, although this can be debatable in cases of extended, complex sources. For example, the 16 observations of Cas A are counted as one source. Group 7 sources include only those that are not offs (31), flagged (13), or at the wrong coordinates (28).

[a] Subgroup 2.SE is divided into parts a, b, and c (see text).

PN: prominent emission lines from atomic fine-structure transitions.

PU: similar to PN, but with strong UIR features as well (see below).

U: prominent emission features at 3.3, 6.2, ~7.7–7.9, 8.6, and 11.2 μm commonly described as UIR features. They most likely arise from polycyclic aromatic hydrocarbons (PAHs), although this identification remains controversial. Unless specified otherwise, there are no other strong spectral features. Sources with low-contrast UIR emission difficult to detect when examining full-scan spectra may not be classified as "U." In other words, many sources with fainter UIR features are classified in other groups.

U/SC: a combination of UIR emission features in the blue half of the spectrum and crystalline silicate emission features at 33, 40, and/or 43 μm.

E: no discernible spectral structure, except for the presence of atomic emission lines.

F: featureless spectrum (within the signal-to-noise ratio).

W: the continuum emission peaks at ~6–12 μm, usually with apparent silicate absorption at 10 μm. The "W" stands for Wolf-Rayet, since these spectra are always produced by Wolf-Rayet stars or R Corona Borealis variables.

M: miscellaneous spectra. Most of these objects have distinct features but could not be placed in any of the other existing categories, even with a "p" suffix. Objects that clearly belong in the parent group but are too noisy to classify further into a subgroup also appear here.

Because some spectral characteristics occur across a broad range of temperature, the same level 2 subgroup description can appear in different level 1 groups. Table 4 summarizes the occurrence of each level 2 subgroup within the level 1 groups.

3.3. *Group Descriptions and Sample Spectra*

Each group of level 1 spectra separates into several subgroups, often including a subgroup for peculiar or noisy spectra that defied attempts to unambiguously place them elsewhere. The figures illustrate sample spectra for each subgroup. Spectral classifications and source types are taken from the literature or from SIMBAD.

3.3.1. *Group 1: Naked Stars*

The naked stars fall into several easily distinguished subgroups based primarily on the presence or absence of molecular absorption bands. These include ordinary stars (1.N), oxygen-rich stars (1.NO), carbon-rich stars (1.NC), and emission-line stars (1.NE). An additional subgroup (1.NM) includes sources whose SEDs are dominated by photospheric emission but are too noisy or otherwise too peculiar to place with confidence in one of the main subgroups.

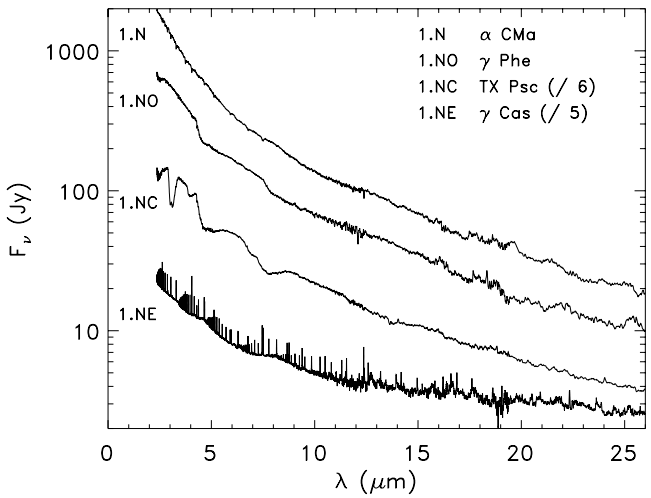

FIG. 1.—Typical spectra from group 1. Numbers in parentheses after the object name indicate the scaling factor used to make the plots.

Figure 1 presents examples of each subgroup, described as follows:

1.N: these stars include the main-sequence stars with no molecular bands in their spectrum. A combination of a simple Engelke function (Engelke 1992) and narrow atomic absorption features (primarily hydrogen recombination lines) accurately describes the spectrum. MK classifications of stars in this subgroup range from O9 V (ζ Oph) to K0 Iab (α UMi).

1.NO: these stars show broad absorption features in their spectra from the CO overtone (maximum absorption $\sim$2.5 μm), a blend of the SiO overtone (4.2 μm) and the CO fundamental (4.6 μm), and the SiO fundamental (8 μm). Additionally, a complex set of narrow absorption features appears at $\sim$3–4 μm. Most of these sources are K and M giants and supergiants with C/O ratios less than unity, although there is one F dwarf and two S stars.

1.NC: these stars show several molecular absorption bands indicative of a carbon-rich photosphere, including narrow bands at $\sim$2.5 (attributed to CO, CN, and C_2) and 3.1 μm (HCN and C_2H_2) and broad bands at $\sim$5 (C_3, CO, and CN), 7–8 (HCN, C_2H_2, and CS), and 14–15 μm (HCN and C_2H_2) (e.g., Goebel et al. 1978, 1980; Aoki, Tsuji, & Ohnaka 1998, 1999).

1.NE: these stars are emission-line stars. Numerous hydrogen recombination lines appear in emission. Recombination lines from helium (Hony et al. 2000) or fine-structure lines from, for example, [Fe II] and [Ni II] (Lamers et al. 1996) may also be present. In some sources, Balmer-like jumps for the infrared series, such as the Humphreys jump 6–∞ near 3.4 μm, produce discontinuities in the continuum (Hony et al. 2000).

A. M. Heras et al. (2002, in preparation) have classified 1.N and 1.NO sources in more detail, reaching level 3 for $\sim$40 sources. They distinguish subclasses of stars with (1) only strong H lines, (2) strong CO absorption and no SiO, (3) strong CO and SiO absorption bands, and (4) strong CO and SiO features plus the H_2O bending mode feature. The strength of the molecular features increases with decreasing temperature and, consequently, later MK class. They also find that the strengths of the infrared bands are well correlated with each other.

3.3.2. *Group 2: Stars with Dust*

Group 2 includes sources with SEDs dominated by the stellar photosphere but also influenced by dust emission (Fig. 2). The nature of the spectral contribution from the dust in the mid-infrared (typically $\sim$10–11 μm) determines the subgroup. The dust properties are usually consistent with the photospheric features in the near-infrared. Most of the sources show oxygen-rich dust emission (SE), and we have separated these spectra into three subgroups based on the shape of the spectral emission feature in the 10–12 μm region analogous to classes defined by LML and SP. The subgroups are described as follows:

2.SEa: these spectra show a broad emission feature peaking at $\sim$12 μm. The dust emission is usually weak, so the spectra resemble those in subgroup 1.NO. The LML system classifies these as "broad" spectra, and the SP system classifies them as SE1–3. This broad feature arises from amorphous alumina dust (Onaka, de Jong, & Willems 1989; Lorenz-Martins & Pompeia 2000). A weak 20 μm silicate feature is usually present, as well as a complex of absorption bands at $\sim$3 μm (from rovibrational H_2O transitions and a broad, deep OH transition). Some sources show the well-known 13 μm emission feature, often associated with narrow CO_2 emission bands at 13.87, 14.97, and 16.28 μm (Justtanont et al. 1998). Roughly 15% of the SEa sources have particularly weak dust emission. A. M. Heras et al. (2002, in preparation) note that one of these, V Nor, has anomalous mid-infrared properties relative to its optical classification, probably the result of an unrecognized thin dust shell.

2.SEb: the SP system describes these spectra as "structured silicate emission" (SE3–6), while the LML system would classify them as "S," "3-component," or "Sil++." These spectra have 10 μm dust features due to amorphous silicates, but they also show a secondary peak to the emis-

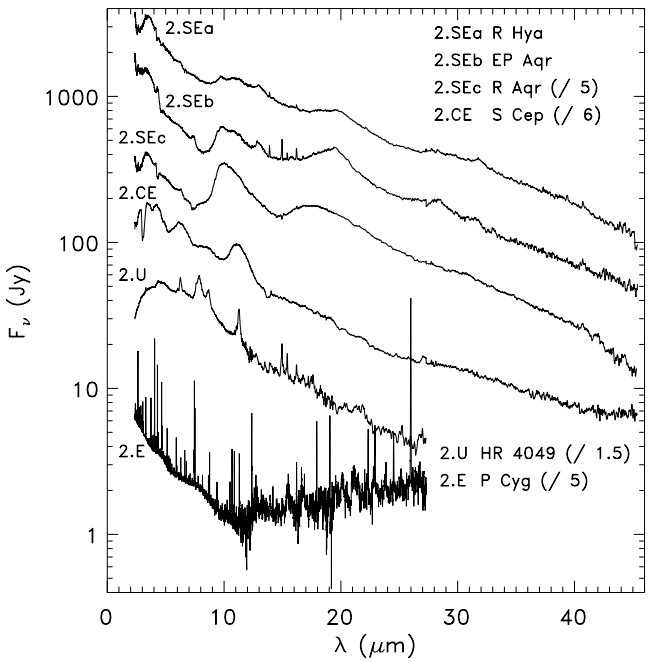

FIG. 2.—Typical spectra in group 2. The 2.U and 2.E spectra are truncated at 27.5 μm (through band 3D) as a result of poor signal-to-noise ratio in bands 3E and 4.

sion at ~11 μm, and they often have a 13 μm feature as well (with associated CO_2 bands). The 18–20 μm feature tends to have a moderate strength, and the H_2O feature at 3 μm in 2.SEa and 1.NO sources is also present, although with less influence from OH. The spectral structure at 10 and 11 μm may arise from a mixture of amorphous alumina or silicate grains (Lorenz-Martins & Pompeia 2000) or from optically thick but geometrically thin shells of pure amorphous silicates (where the emission feature has begun to self-absorb; Egan & Sloan 2001).

2.SEc: these sources have strong silicate emission features with peaks at 10 and 18 μm. A few sources also show the 13 μm feature. The LML system classifies these as "Sil" or "Sil+," and the SP system describes them as "classic silicate spectra" with SE indices of 6–8. The photospheric absorption bands shortward of 10 μm are often complex.

2.CE: these spectra have a strong emission feature at ~11.5 μm due to SiC dust emission. Photospheric features include bands at 2.5 and 3.1 μm attributed to HCN and C_2H_2 and at 4.3–6.0 μm attributed to CO and C_3 (e.g., Hron et al. 1998; Jørgensen, Hron, & Loidl 2000). The complexity of the emission and absorption features shortward of 10 μm makes it difficult to determine the continuum level in this wavelength region.

2.C/SE: these spectra have carbon-rich photospheric features but the oxygen-rich silicate emission feature at 10–12 μm. Two known silicate carbon stars, V778 Cyg and W Cas, are tentatively joined in this subgroup by RZ Peg.

2.U: the two sources in this category show stellar photospheres with superimposed UIR emission features. The photospheric spectrum for XX Oph resembles the 1.NO sources. The photosphere for HR 4049, an unusual low-metallicity, high mass-loss, post-AGB star (e.g., van Winckel, Waelkens, & Waters 1995 and references therein), is unique in the SWS database.

2.E: these sources show emission lines on a photospheric SED, with possible weak dust emission features in the 12–20 μm range. The exception is WR 147, which may have silicate absorption in its spectrum (Morris et al. 2000).

2.M: this subgroup includes miscellaneous spectra that contained dust emission but could not be assigned to another subgroup, primarily as a result of a poor signal-to-noise ratio in the ~10–12 μm region.

3.3.3. *Group 3*

Emission from warm dust dominates the SEDs of group 3; this dust emission usually arises from a circumstellar shell. The spectra peak shortward of ~20 μm, usually at 10–15 μm, but they show little or no contribution from a stellar photosphere. Like the previous groups, the carbon and oxygen sequences are quite distinct, as Figure 3 illustrates. The subgroups are described as follows:

3.SE: these sources show silicate emission at 10 μm superimposed on the thermal continuum from the dust shell. The dust emission features resemble the classic silicate features in subgroup 2.SEc (at 10 and 20 μm), but with no photospheric emission present as a result of the optically thicker dust shell. Three sources, all symbiotic novae, show several forbidden emission lines (3.SEe), notably [Ne VI] at 7.65 μm, [Ne V] at 14.32 and 24.32 μm, and [O IV] at 25.89 μm. Three other sources have peculiar spectra (3.SEp) with a weak or missing 20 μm emission feature; two of these are S stars. The

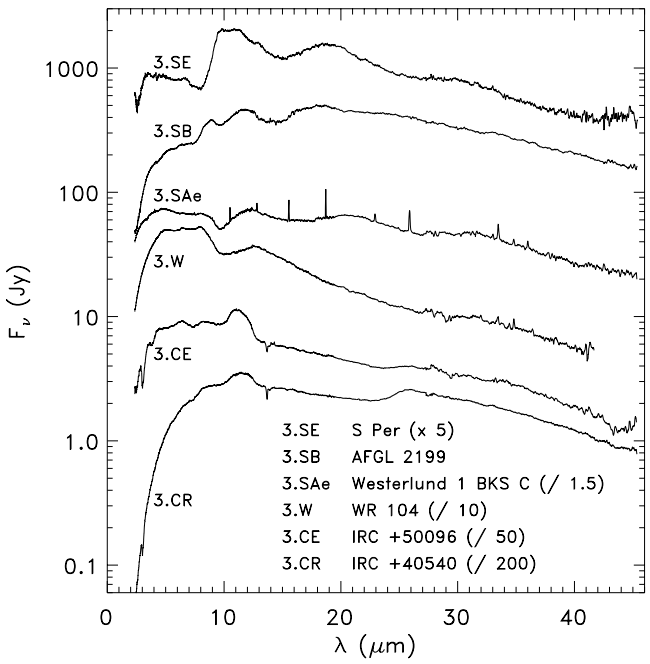

FIG. 3.—Typical spectra in group 3

more typical 3.SE sources tend to be AGB sources, OH/IR stars, or supergiants, although three of these 14 are pre–main-sequence Ae or Be stars.

3.SB: these spectra arise from optically thick shells; self-absorption of the silicate dust has shifted the 10 μm feature closer to 11 μm. The SEDs peak at ~18–19 μm, and some sources show crystalline silicate features longward of 30 μm. The sources are associated with the AGB or OH/IR stars.

3.SAe: this unusual subgroup shows a 10 μm absorption feature and bright emission lines from [S IV] at 10.5 μm, [Ne II] at 12.8 μm, [S III] at 15.6 μm, [Fe III] at 22.9 μm, and [S III] at 33.5 μm. The 20 μm silicate emission feature is more rounded than in the SE and SB spectra and appears at a slightly longer wavelength. Both sources are young or pre–main-sequence Be stars.

3.CE: these spectra resemble the 2.CE subgroup, showing an emission feature ~11.5 μm from SiC, but dust absorption obscures the photospheric absorption features from molecular bands that dominate the near-infrared wavelengths of the 2.CE and 1.NC spectra. Most of the sources show a narrow and often deep C_2H_2 absorption band at 13.7 μm.

3.CR: these sources are cooler analogs of the 3.CE sources. The 11.5 μm SiC emission feature still dominates, and the C_2H_2 absorption band at 13.7 μm is still prominent, but other emission features also appear, usually in the 26–30 μm region and sometimes at 8 μm. IRC +10216 is the brightest of these sources; radiative transfer modeling of its spectrum suggests that amorphous carbon dominates the SiC dust component (~90%–95%; e.g., Martin & Rogers 1987; Sloan & Egan 1995). The optical efficiency of amorphous carbon follows a λ^{-1} relation in the mid-infrared, mimicking a blackbody of lower temperature than the actual dust temperature (Martin & Rogers 1987).

3.W: the spectra of these sources peak at ~6–8 μm. Most show strong silicate absorption features at 10 μm similar to the 4.SA feature. Except for the 10 μm feature, the spectra are nearly featureless and have little similarity to sources in

any other subgroup. All members are either Wolf-Rayet or R Corona Borealis stars.

3.3.4. *Group 4*

Dust emission dominates the SEDs of group 4, and the dust temperature is cooler than in group 3, with the spectra peaking at wavelengths between ~20 and ~40 μm. The photospheric contribution is generally negligible. Several of the subgroups in group 4 are analogous to those in group 3, but with significantly cooler dust. As in the warmer groups, the carbon and oxygen sequences are quite distinct. The carbon-rich spectra continue in relatively tight groups, whereas the oxygen-rich dust spectra form a rather heterogeneous group. Finding distinct and self-consistent subgroups for these spectra has proven difficult, and finding subgroups populated by uniform samples has proven impossible. Figure 4 shows sample spectra from group 4. The subgroups are described as follows:

4.SE: these sources show an emission feature from amorphous silicates at 10 μm superimposed on emission from a cool dust shell. As in subgroup 3.SE, the contrast varies significantly from one source to the next. Most of the SEDs peak around 20–25 μm, although in three sources the peak is near 30 μm. Of all the subgroups in group 4, this is the most difficult to characterize, in part because of the low signal-to-noise ratio of many of the spectra. The specific shapes

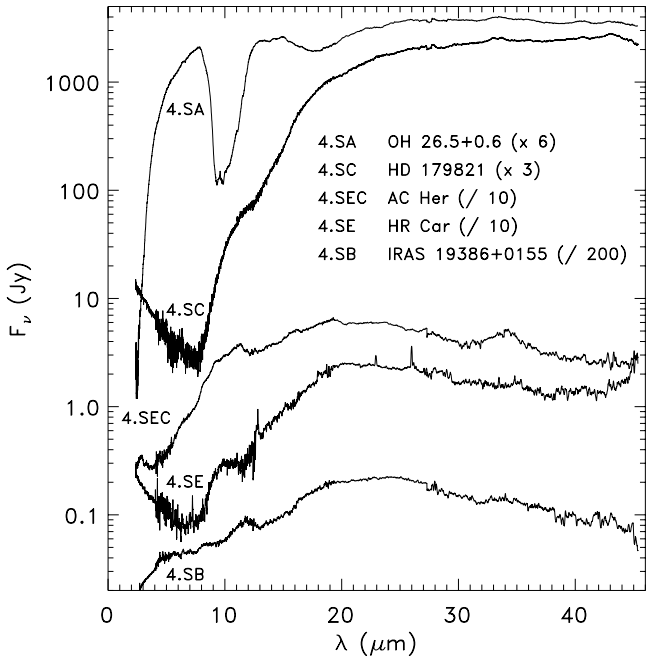

FIG. 4*a*

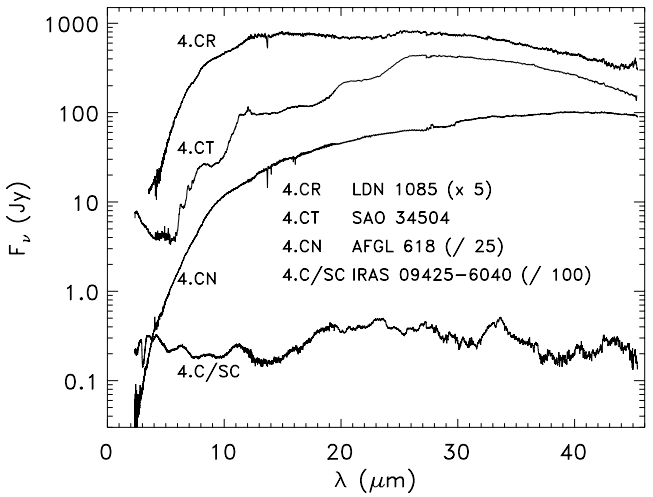

FIG. 4*b*

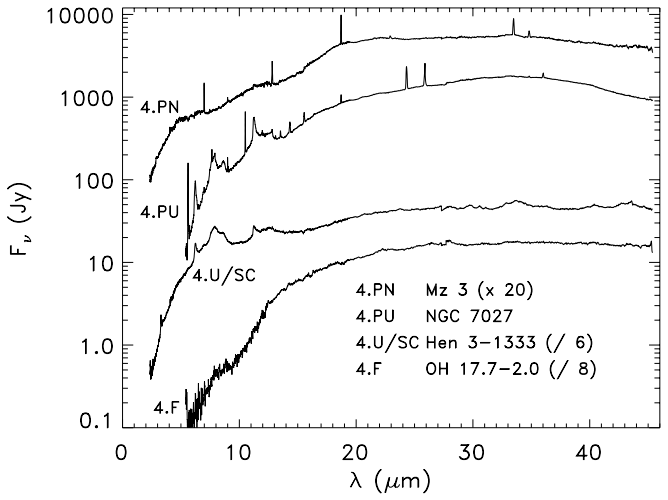

FIG. 4*c*

FIG. 4.—Typical spectra for group 4. (*a*) Oxygen-rich sources, arranged in a possible evolutionary sequence (§ 4.3.2). (*b*) Carbon-rich sources. The spectrum for 4.CR is truncated at lower wavelengths as a result of poor signal-to-noise ratio. (*c*) Spectra for 4.PU and 4.F are truncated at lower wavelengths as a result of poor signal-to-noise ratio.

of the SED and the 10 μm silicate feature differ among the sources. Some spectra, often with bluer SEDs, show forbidden emission lines (the specific transitions vary substantially from source to source). Most 4.SE sources have optical spectral classes of Be, Ae, or Fe or are described as PNs. While more than half of the sources are post–main-sequence, several are Herbig Ae/Be stars or related pre–main-sequence objects.

4.SEC: these sources show prominent crystalline silicates in at least two of three positions, $\sim$11, 23, and 33 μm. The 11 μm emission feature may be weak, in which case the usual amorphous feature at 10 μm appears to be broadened, or it may dominate, producing a strong, sharp peak at 11 μm. Additional crystalline silicate features may also be present at 19 and 43 μm. Like 4.SE, this subgroup includes a heterogeneous collection of sources, but only three of the 11 objects are clearly identified as pre–main-sequence. The rest tend to be young PNs or PPNs; the sample also includes one Mira variable and the hypergiant IRC +10420.

4.SB: the 10 μm silicate feature is in self-absorption, sometimes strongly, and emission features from crystalline silicates may be present at 33, 40, and/or 43 μm, though not strongly. The majority of sources are PNs or PPNs, although one may be a pre–main-sequence Ae star, another is a Be variable, and a third is an AGB source.

4.SA: this subgroup exhibits silicate absorption at 10 μm and sometimes also at 18 μm. Most sources show emission features from crystalline silicates at 33, 40, and 43 μm. Stronger absorption at 10 μm usually occurs with stronger emission from crystalline silicates, especially at 33 μm. The deepest 10 μm absorption features arise from OH/IR stars. Other sources in this subgroup include PPNs and PNs. Two of the three bluest sources are more difficult to characterize and may be pre–main-sequence stars.

4.SC: all sources in this subgroup show crystalline silicate emission features at 33 and 43 μm. Many also show crystalline silicate features at 23 and 40 μm. The source types are somewhat heterogeneous, although PPNs and PNs (especially young PNs associated with Be central stars) dominate. Other sources include Wolf-Rayet stars, OH/IR stars, and one source identified as a pre–main-sequence G star (DG Tau).

4.F: the SEDs of sources in this subgroup basically have no features (greater than the noise), with no silicate emission or absorption at 10 μm or any crystalline silicate emission at longer wavelengths. Three sources do show UIR emission, and one has several nonsilicate absorption features due to ices. Most sources are PNs or OH/IR stars, except for the source with ice absorption, which is a YSO (R CrA [TS84] IRS 2).

4.CR: this subgroup continues the carbon-rich dust sequence (2.CE–3.CE–3.CR) to cooler shells. The SEDs peak at $\sim$28 μm and are broad and nearly featureless, except for the 26–30 μm emission feature and the C_2H_2 absorption feature at 13.7 μm. Extreme carbon stars and carbon-rich PPN candidates dominate the source types.

4.CT: these sources have SEDs with a steplike appearance produced by emission features on a steadily rising red continuum at 8, 11.5, 21, and 26–30 μm. The 21 μm can be prominent, and the SEDs peak at $\sim$30 μm. Unlike the other dusty carbon-rich sources, they do not have the C_2H_2 absorption feature at 13.7 μm. Sources tend to be F or G supergiants sometimes identified as PPN candidates.

4.CN: these sources show features such as the C_2H_2 13.7 μm absorption or the 11.5 μm emission feature, which indicate that they are carbon-rich. The SED peaks at $\sim$40 μm. All of the sources are identified as PPNs, and this subgroup includes the well-known carbon-rich bipolar nebulae AFGL 618 (the Westbrook Nebula) and AFGL 2688 (the Cygnus Egg). The "N" designation stands for "nebula."

4.C/SC: the one source in this subgroup (IRAS 09425−6040) has an unusual spectrum, showing carbon-rich molecular absorption bands in the near-infrared and SiC emission at $\sim$11.5 μm as seen in 2.CE spectra as well as strong crystalline silicate emission features at 33, 40, and 43 μm. Molster et al. (2001) suggest that IRAS 09425−6040 may be in transition to a Red Rectangle–like object (see subgroup 4.U/SC below). Normally, a unique spectrum would belong in a miscellaneous subgroup, but the relation of this spectrum to the more numerous U/SC subgroup suggests that more of these sources may be discovered in future observations.

4.U/SC: the sources in this subgroup combine strong UIR features (at 6.2, 7.7–7.9, 8.6, and 11.2 μm) and strong crystalline silicate emission features (at 33, 40, and 43 μm). The 33 μm feature can be quite prominent and, in the bluer sources, can be accompanied by a 23 μm emission feature also due to crystalline silicates. Most spectra show a possible emission feature at $\sim$28.5 μm, but the poor quality of band 3E makes this identification problematic. All of the sources are PPNs or PNs, with the exception of a single Herbig Ae/Be star (HD 100546).

4.PN: the dominant spectral feature in this subgroup is the presence of strong fine-structure lines superimposed on an SED that peaks in the vicinity of 30 μm. The line-to-continuum ratio can be 5 or greater in some instances. All show, at a minimum, [Ne II] at 12.8 μm and [S III] at 18.7 and 33.5 μm. Other common lines include [Ar II] at 6.99 μm, [Ar III] at 8.99 μm, [S IV] at 10.5 μm, [Ne III] at 15.6 and 36.0 μm, and [Si II] at 34.8 μm, as well as Brα and Brβ. Additional detected lines include [Ne V] at 14.3 and 24.3 μm, [Ne VI] at 7.65 μm, [Ar V] at 7.90 and 13.1 μm, [Ar VI] at 4.53 μm, [O IV] at 25.9 μm, [Mg IV] at 4.49 μm, and [Mg V] at 5.61 and 13.5 μm. Some sources also show weak crystalline silicate features, especially at 33 μm. All but one source are PNs; the exception, IRAS 05341+0852, is a PPN candidate.

4.PU: similar to 4.PN, these sources show strong UIR features in addition to the fine-structure lines. BD +30°3639 shows crystalline silicate emission at 33 μm. Most are PNs, including one PPN candidate. Three sources with fewer, weaker emission lines than the typical PU spectrum are noted as peculiar with the "p" suffix; otherwise, their SEDs and UIR features resemble the other members closely.

4.M: each of the four objects in this subgroup is unique. η Car could be described as the prototypically strange spectrum at all wavelengths. Classification of its SWS data is further complicated by the saturation (and automatic flagging) of most of band 3, the spectral region upon which much of the subgrouping in group 4 is based. AG Car combines a group 1 spectrum (1.NE) in the near-infrared with a group 4 spectrum (possibly 4.PUp) at longer wavelengths. Only a few other objects show this combination of hot photospheric emission with very cool dust. IRAS 21282+5050 has very strong UIR features, most similar to those in the Red Rectangle (HD 44179, 4.U/SC), but has no crystalline silicate emission and a significantly bluer SED than members of the

4.U/SC subgroup. HD 169142 is somewhat similar to the 4.U/SC or PU group in terms of its UIR emission and SED but has no evidence for crystalline silicates or emission lines in its admittedly weak, noisy spectrum.

3.3.5. *Group 5*

Objects in group 5, whose SEDs are still rising through the end of band 4, have the coolest dust emission in the database. The subgroups trace the presence of silicate emission or absorption, narrow emission lines, UIR features, and absorption features. Figure 5 shows sample spectra for group 5. The subgroups are described as follows:

5.SE: these sources show broad silicate emission features at $\lambda \sim 9$–11 μm. One (AB Aur) also shows UIR emission features. All but one are young, Herbig Ae/Be (or Fe) stars. The single evolved source, HD 101584, a PPN candidate, could be a cooler version of the 4.SE sources, or it may actually be a young object misclassified as old.

5.SA: sources in this subgroup show a broad silicate absorption feature at $\lambda \sim 9$–11 μm. Other absorption features often present include bands from CO_2, CO, and H_2O. A few also show UIR emission features or weak atomic fine-structure lines ([Ne II], [S III], or [Si II]). Almost all sources are YSOs or in star-forming regions. The six (out of 50) that are not YSOs are probably OH/IR stars. Four of the sources in this class with emission lines (5.SAe) are Galactic center objects.

5.F: these sources show no strong features superimposed on an SED that rises steadily to the red. Some sources in this class may be better placed in other classes, but because the red end of the spectrum is so strong, any structure at $\lambda \lesssim 15$ μm is not visible on the self-scaled plots used for classifying. Three of the sources are evolved; the rest are young.

5.U: these sources have moderate to strong UIR features but no atomic fine-structure lines. Only one source is considered evolved (Wray 15-543, thought to be a PPN candidate); the rest are young.

5.UE: these sources have moderate to strong UIR features and strong atomic fine-structure lines. The majority of the sources are young; a few are thought to be evolved (PNs).

5.E: these sources have strong atomic fine-structure lines but little or no UIR emission. The composition of this subgroup is similar to 5.UE: mostly pre–main-sequence stars with a few PNs.

5.PN: these sources have very strong, numerous atomic fine-structure lines. Crystalline silicate emission is often present in the $\lambda \sim 30$–45 μm range, and at least two show UIR emission. All sources are evolved (PNs).

5.M: the weak signal and poor signal-to-noise ratio of these spectra hide any identifying features that would help to place them in a different subgroup.

4. DISCUSSION

4.1. *Calibration Issues and the Classifications*

As mentioned in § 2.2, the browse products used to classify most of the spectra did not fully correct for flux discontinuities between bands. The most challenging normalization problems occur between bands 2C and 3A, at $\lambda \sim 12$ μm, and between bands 3D, 3E, and 4, at $\lambda \sim 26$–30 μm. We discuss them briefly here to the extent that they influence the classification effort.

Spectra in group 2 are most sensitive to discontinuities and memory effects near 12 μm because the shape of the emission and absorption features in the 10–12 μm region serve as the primary features for classification into the sub-

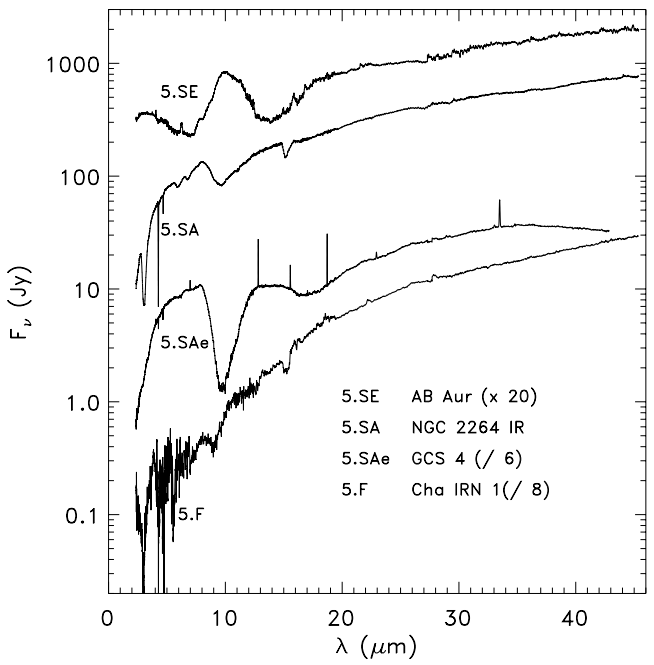

FIG. 5*a*

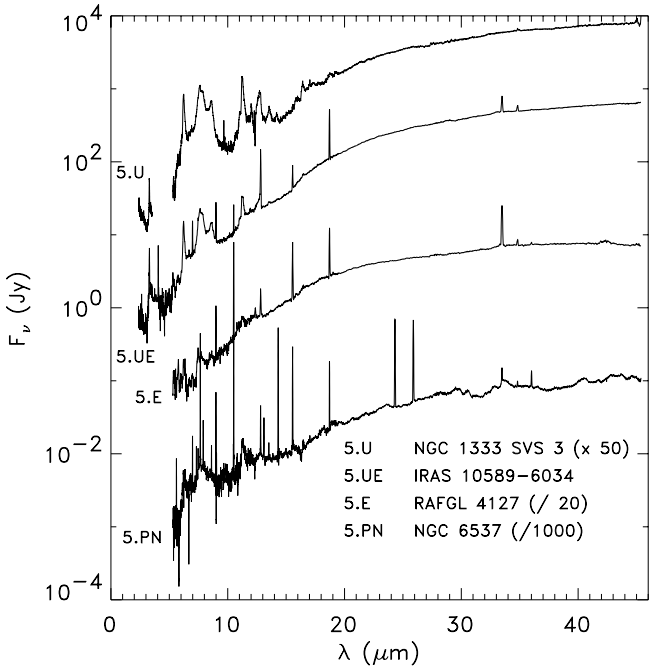

FIG. 5*b*

FIG. 5.—(*a*) Typical spectra in group 5. (*b*) In 5.U, band 2A is omitted as a result of poor signal-to-noise ratio. Likewise, the spectra for 5.E and 5.PN are truncated at shorter wavelengths.

groups. If the flux discontinuity is simply related to a gain difference between bands, normalization during reprocessing (if needed at all) would simply scale band 3A to match 2C without changing the basic shape of any features present. If the discontinuity results from memory effects, however, it is more problematic. Even with the *dynadark* correction and normalization some error may remain in the shape of the spectrum. Fortunately, this problem does not compromise the classification of a spectrum as oxygen- or carbon-rich, although it might cause a spectrum to be (mis)-classified as 2.SEa instead of 2.SEb, for instance.

Normalization of bands 3D, 3E, and 4 is complicated by a light leak and by the unreliability of 3E. Most spectra show a smooth shape with a roughly constant slope from band 3D through band 3E and into band 4, which allows a straightforward normalization of these bands to each other. However, spectra with structure near 26 μm present more of a problem, since the changing slope of the spectrum makes extrapolation across band 3E difficult. This problem affects the carbon-rich sources in groups 3 and 4 most significantly and limits our confidence in the shape of the emission feature in the 26–30 μm region. In the browse product spectra produced from OLP 7.1, the normalization of the segments makes the 26–30 μm feature appear narrow and peaked around $\sim$25–29 μm. Applying our normalization algorithm to data in OLP 10.0 broadens the feature to $\sim$25–34 μm. The literature tends to refer to this feature as the 30 μm emission feature, possibly attributable to MgS (Goebel & Moseley 1985; Begemann et al. 1994). With the current uncertainties in calibration, we are unable to definitively address this issue.

To date, no model has been developed to correct the memory effects in band 4. The entire shape of band 4 can be compromised, and, in terms of the spectral classification, this influences whether a spectrum is classified in group 4 or 5. For example, a spectrum could be misclassified as a 4.PN instead of a 5.PN because the spectrum appears to have turned over in band 4 when it is actually still climbing. The memory effect in band 4 can also influence our ability to recognize crystalline silicate features, especially at 40 and 43 μm. These features could be washed out when the two scan directions are combined because of the difference in flux levels between them. As with the other issues raised here, the band 4 memory effect should have a limited impact on the classifications.

Despite these issues, the basic classification scheme and the grouping of the spectra should prove robust. The movement of a few spectra from CR to CE or from group 4 to 5 will not change the overall nature of the database or the existence of any of the evolutionary patterns discovered therein (§§ 4.3.1–4.3.3).

4.2. *Comparison with IRAS Classifications*

Although we are dealing with a nonuniform database (§ 2.1.2), we can still compare our classifications with the LRS classes (*IRAS* Explanatory Supplement 1988) and the classes of Kwok et al. (1997). Only the subset of SWS sources with LRS classifications (379 sources) or Kwok et al. (1997) (567 sources) classifications can be considered, so the numbers quoted below will not be the same as those given for each subgroup in Table 4. In addition, recall that for LRS class 1n, $n = 2\beta$, where β is the spectra index:

$$F_\lambda \propto \lambda^{-\beta} . \quad (1)$$

Thus, when $\beta = 4$, the spectrum behaves as a pure Rayleigh-Jeans tail and is in LRS class 18. Sources with low-contrast dust mimic lower spectral indices and receive lower LRS characterizations. For example, LML and SP showed that many sources in LRS classes 13–16 show low-contrast alumina-rich dust in their spectra.

4.2.1. *Similarities*

Group 1, the dust-free stars, corresponds well to the LRS classes 17–19. Of the 60 objects in group 1 with LRS classifications, 54 are in LRS classes 17–19, with 39 in class 18. Of the 2.SEa sources, with low-contrast dust, 81% of the 53 sources are in LRS classes 13–16, as expected. Similarly, the oxygen-rich dust sequence, described in § 4.3.2, should begin in the 2n range and progress to the 3n range, where 2n corresponds to silicate emission and 3n to silicate absorption. Nearly 90% of the 67 objects in subgroups 2.SEb, 2.SEc, and 3.SE have LRS classes 2n. The sources in 3.SB, the self-absorbed subgroup, are split between 2n and 3n, and 11 of 12 sources in 4.SA are 3n or 7n (recall that 7n is the red counterpart of 3n). In the carbon-rich sources, 31 of 37 sources in subgroups 2.CE, 3.CE, and 3.CT have LRS = 4n, the carbon-rich LRS class. Only about one-third (14 of 41) of the PN subgroups 4.PN, 4.PU, and 5.PN have LRS classifications, but those that do tend (11 of 14) to be 9n, that is, red objects with emission lines but no detected 11.3 μm UIR feature. For the young, red sources in groups 4 and 5, even fewer, $\sim$25%, have LRS classifications, so small numbers make valid comparisons problematic. Still, most of those with LRS data in our SA or SE subgroups do have silicate absorption or emission LRS classifications.

A comparison of our classifications with those of Kwok et al. (1997) shows comparable similarities. For example, 37 of the 40 sources with their class C, for carbon-rich, are in one of our carbon-rich subgroups (mostly 2.CE). More than 80% of their A (10 μm absorption) sources are in our SA or SB subgroups, and more than 90% of their E (10 μm emission) sources are in our silicate emission subgroups. Almost 90% of their S (stellar) sources are in group 1, our naked star category.

4.2.2. *Distinctions*

While the overall correspondence between our classifications and those from LRS-based schemes is reasonable, there are a number of important differences. For instance, misidentification of UIR features as silicate absorption occurred in the LRS classifications as a result of the low spectral resolution and bandwidth. This is largely avoided in the SWS database because of the higher spectral resolution and especially the expanded bandwidth. The extended wavelength coverage allows confirmation of suspected 7–11 μm UIR features with those at 6.2 and 3.3 μm that were outside the LRS range.

It was mentioned above that most of the 4.SA and 5.SA sources (24 of 27) were in LRS classes corresponding to silicate absorption. However, 17 of those sources were 3n, with ostensibly blue SEDs. Characterizations of 7n would have been more correct, but the short-wavelength cutoff of only 7 μm presumably prevented an accurate assessment of the overall SED. In the 5.UE group, 25 sources had red LRS

characterizations, but less than half (10) were 8*n*, the UIR + emission-line class. Lack of sensitivity of the LRS precluded the detection of UIR bands in some sources, while the limited spectral range caused the confusion of UIR bands and silicate absorption in others.

Examination of the carbon-rich classes and ostensibly carbon-rich objects further illustrates the limitations of the old LRS classifications when dealing with SWS data. One source, AFGL 2287, was classified as carbon-rich in all three LRS-based schemes but is classified by us as self-absorbed silicate emission (3.SBp). In the limited spectral range of the LRS data, self-absorbed silicates can appear similar to carbon-rich spectra (Walker & Cohen 1988). However, with the SWS, AFGL 2287 can be seen to have none of the other features typical of carbon-rich sources such as the absorption features at 13.7 or 3 μm. Seven other sources were classified as carbon-rich in the LRS atlas but as oxygen-rich by AutoClass and Kwok et al. (1997). With the high-quality data from SWS, we can confirm that they are indeed oxygen-rich.[12]

As an example of a discrepancy in the opposite sense, only one of our 4.CR sources has a carbon-rich LRS class, while most of the rest (eight of 11) are classed as 21–23, low-contrast silicate emission. The AI classifications also mistook most of 4.CR (nine of 10) for oxygen-rich (ζ4) because of the limited spectral range on which the classifications were based. Of the 31 objects observed with SWS that SIMBAD lists as carbon stars, only two (FI Lyr and CIT 11) are in noncarbon KSPW subgroups; four more are in group 7 or flagged, so 25 of 27 agree with SIMBAD. The LRS scheme, on the other hand, has only 16 of 24 sources with 4*n* or 04 designations. Again, the superior sensitivity and spectral range of SWS enabled the proper classification of these sources as carbon-rich.

The LRS 4*n* classes base the second digit on the strength of the 11.5 μm silicon carbide feature. However, nothing in the LRS classification indicates the shape of the underlying continuum for carbon-rich objects. Thus, sources as dissimilar as RY Dra (2.CE) and IRAS 22303+5950 (4.CR) possess the same LRS classification 41 because both have weak 11.5 μm features (Fig. 6). LRS class 44 contains both W Ori (2.CE) and IRC +50096 (3.CE) despite their distinctly different underlying SEDs. There simply are *no* appropriate categories in the LRS scheme in which to place *any* of the carbon-rich sources in our groups 3 and 4 without loss of significant information about the spectra.

Similarly, placing all of our group 1 naked stars into 1*n* would also cause the loss of important information about the photospheric chemistry (1.NO vs. 1.NC) or the presence of emission lines (1.NE). Other KSPW classes with no good LRS counterparts include 2.E, 2.U, 2.C/SE, 4.SC, 4.U/SC, 4.SEC, and 6.

Other LRS classes also mismatched sources, as Figure 6 shows. These disparate sources were placed in the same LRS classes because of the limited spectral range of the LRS and small number of features considered in that classification scheme. Table 5 compares the KSPW classes to the LRS classes. The second column lists the KSPW classes that are well matched to an LRS class as defined in the *IRAS* Explanatory Supplement (1988), for example, 1.N and the

[12] They are ST Her (2.SEa), FI Lyr (2.SEa), Z Cas (2.SEap), π^1 Gru (2.SEa), AD Per (2.SEa), AFGL 2199 (3.SB), and AFGL 1992 (3.SB).

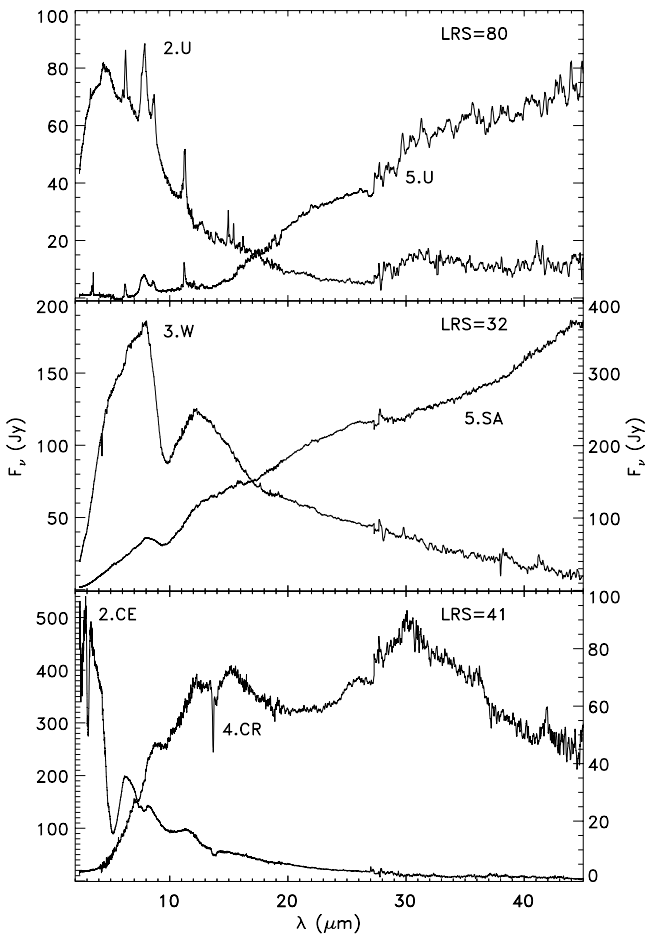

FIG. 6.—Comparison of spectra with the same LRS class but different KSPW classes. *Top:* LRS = 80 (UIR emission); HR 4049 2.U and HD 97048 5.U (smoothed). *Middle:* LRS = 32 (blue SED plus silicate absorption); WR 112 3.W and V645 Cyg 5.SA. *Bottom:* LRS = 41 (C-rich); RY Dra 2.CE and IRAS 22303+5950 4.CR.

1*n* class. The third column lists our groups that could be placed in an LRS class, but only with information lost, such as 2.C/SE in 2*n* or 4.U/SC in 8*n*. The last column lists the other KSPW groups in which the LRS classes actually appear but are not well suited to each other. Application of the LRS scheme to classify the SWS database would have essentially ignored the additional information gained from the larger bandwidth, higher spectral resolution, and greater sensitivity of SWS.

4.3. *Clarifying Evolutionary Patterns*

4.3.1. *The* CO *Paradigm*

The search for patterns and relations among the infrared spectral classifications identified here must first consider the observed dichotomy between carbon-rich and oxygen-rich dust chemistry. In evolved stars, the chemistry of the dust depends on the C/O ratio of the material ejected from the envelope. The formation of CO molecules will exhaust the less abundant of carbon or oxygen, leaving the other element available to form molecules that serve as seeds for dust formation. This CO paradigm works admirably well. In only a few cases does the chemistry of the stellar photosphere differ from that of the dust, and most of these cases probably arise within binary systems. For example, the sili-

TABLE 5
KSPW versus LRS Classifications

LRS	KSPW		
	OK	Information Lost	Mismatch
		"Blue"	
1*n* featureless.....	1.N	1.NC, 1.NO (1.NE)	2.CE, 2.M, 2.SEa, 2.SEb, 3.CR, 3.SA, 3.W, 4.CR, 4.SB, 4.U/SC, 6
2*n* 10 μm emission	2.SEa, 2.SEb, 2.SEc, 3.SB, 3.SE	2.C/SE	1.N, 2.CE, 4.CR, 4.SE, 4.SEC
3*n* 10 μm absorption...	2.M, 3.SB, 3.W (3.SA)		1.NC, 2.SEb, 4.SA, 4.SB, 4.SC, 5.SA, 5.U, 6
4*n* carbon-rich.....	2.CE	3.CE, 3.CR, 4.CR (4.CN, 4.CT, 4.C/SC)	2.SEa, 3.SB, 4.SB
		"Red"	
5*n* featureless.....	4.F (5.F)	(4.SC)	2.SEa, 3.CR, 4.C/SC, 4.SB, 5.SA, 5.UE
6*n* 10 μm emission	3.SE, 4.SE, 5.SE (4.SB)	4.SEC	2.SEc, 4.CN, 4.SC
7*n* 10 μm absorption...	4.SA, 5.SA (3.SA, 4.SB)	4.U/SC	4.F, 4.CN, 4.CT, 4.SC, 5.U, 5.UE
8*n* UIR + lines.....	4.M, 4.PU, 5.U, 5.UE	2.U, 4.PN	
9*n* lines only	4.PN, 5.E, 5.PN	4.PU, 4.SEC, 5.F, 5.SA, 5.UE	

Note.—KSPW classes in parentheses could reasonably have appeared in a given LRS class but did not.

cate carbon stars (2.C/SE) show carbon-rich photospheric features and oxygen-rich dust. In these sources, the dust emission may arise from a disk around an unseen companion that trapped mass lost from the primary before it evolved into a carbon star (see Yamamura et al. 2000 for a recent study of the SWS spectrum of V778 Cyg and a discussion of competing models).

Circumstellar dust shells form in relatively pure environments, but interstellar dust represents a mixture of material ejected by many generations of evolved stars with a wide variety of progenitor masses. Since oxygen-rich dust shells outnumber carbon-rich dust shells, oxygen-rich dust dominates in the interstellar medium. This means that an oxygen-rich dust spectrum can arise in either a pre–main-sequence or a post–main-sequence environment, but carbon-rich spectra will only appear in post–main-sequence objects.

4.3.2. *Oxygen-Rich Dust Emission*

The oxygen-rich post–main-sequence objects can be organized along the sequence AGB source → OH/IR source → PPN → PN. This sequence assumes that as the average oxygen-rich star evolves up the AGB, its mass-loss rate increases, eventually enshrouding it so deeply within its circumstellar dust shell that it disappears completely from the optical sky. This first stage of development is well documented. Jones et al. (1990), in a study of variable AGB sources identified by the Air Force Geophysics Laboratory (AFGL) infrared sky survey (Price & Murdock 1983), showed that as Mira variables evolve to OH/IR stars, the period of variability and mass-loss rate steadily increase as the infrared colors progressively redden. They showed photometrically that this evolution transformed the silicate emission feature at 10 μm to a deep absorption feature. Lloyd Evans (1990) illustrates this change spectroscopically with LRS data in his Figure 3.

Examining the composition of each subgroup (in terms of the fraction represented by AGB sources, OH/IR stars, PPNs, and PNs) helps to organize the spectral subgroups defined in our classification system into an evolutionary sequence. In some cases, the composition of a subgroup is obvious; in others the small sample sizes and the inherent selection effects of the SWS database limit the usefulness of this method.

The initial steps are relatively straightforward to interpret. A star on the early AGB will appear as a naked star with absorption bands from CO and SiO (1.NO). Reinterpreting Figure 8 of Sloan & Price (1995) in terms of the subgroups defined here, the shift from 1.NO to 2.SE occurs between (time-averaged) spectral types of M4 and M5. This marks the onset of significant mass loss and dust formation, but the detailed evolution through the various classes of silicate emission (broad, structured, and classic) is more difficult to trace. SP found few correlations between spectral type, variability class, and the shape of the silicate dust spectrum. They suggested that the formation of multiple shells might cloud the picture and that the shape of the spectrum might depend on photospheric C/O ratio, which would imply that dredge-ups of processed material from the stellar interior might determine the shape of the infrared dust features. Detailed analysis of the shape of the silicate feature and related features, such as the CO_2 lines and the 13 and 19.5 μm bumps, in the 2.SE subgroups may shed further light on this subject (Sloan et al. 2001a).

As the dust contribution grows to dominate the stellar spectrum, the spectrum will shift from group 2 to 3 (3.SE). It will then develop into a 3.SB spectrum as the optical depth of the silicate dust increases and drives the 10 μm feature into self-absorption. The 3.SE sources are a mixture of M stars on the AGB, M supergiants, and optically enshrouded OH/IR stars. The 3.SB sources are more evolved, with later spectral types and longer periods of variability. All of the sources in 3.SE were initially discovered in infrared surveys, and all show OH masers. The lack of a single source with a 2.SB spectrum suggests that the transition to self-absorption occurs in group 3.

Evolution continues from 3.SB to 4.SA, where the silicate feature goes into full absorption and the SED becomes redder. The sources in this group are associated with OH/IR stars, many of them Mira variables, and PPNs. The transition to SA does not occur within group 3 because all of the 3.SA spectra are associated with pre–main-sequence sources. It also does not appear to occur frequently within group

4, as most of the 4.SB sources appear to be much more evolved PNs. Rather, the transition from SB to SA appears to coincide with the transition from group 3 to 4.

The stages following 4.SA are much less clear. Ultimately, the high mass-loss rates associated with the end of the AGB-OH/IR phase will strip the envelope from the core, producing a PPN. As the remnant shell expands and thins, revealing the ionized central regions, the source becomes a PN. How does this process manifest itself into the subgroups not yet included in the sequence (4.SB, 4.SE, 4.SEC, and 4.SC)? All four subgroups show roughly the same percentage of clearly identified PNs (58%–60% of the sample, excluding high-mass objects and pre–main-sequence objects), but only 4.SC and 4.SEC include any sources identified as OH/IR stars or still on the AGB. Because of this, we suspect that 4.SC and 4.SEC precede 4.SE and 4.SB on a typical evolutionary path.

Waters et al. (1996) first identified crystalline species of silicates in the spectra of circumstellar dust shells associated with evolved stars using data from the SWS. They noted that the crystalline features do not appear until the color temperature of the shell has decreased to ~300 K. Further study of SWS data by Sylvester et al. (1999) relates the presence of crystalline features with the optical depth at 10 μm. They suggest that crystalline silicates do not appear until the mass-loss rate has crossed a certain threshold. Thus, as mass-loss rate increases, absorption strength at 10 μm grows stronger, and color temperature reddens, a typical source will evolve to SA and then to SC.

Most of the sources in subgroups 4.SC, 4.SEC, 4.SB, and 4.SE appear in the upper middle of the H-R diagram (spectral class B, A, F, and G, usually with emission lines, luminosity class I–II). Whatever their precise order, most or all of the post–main-sequence sources with these classes of spectra are obviously in transition from the AGB or red supergiant phase to later stages of evolution. It is likely that the difficulty in ordering these subgroups results from the wide range of stellar masses that can produce oxygen-rich dust shells (from less than 1 $M_\odot$ to beyond 50 $M_\odot$). The more massive stars do not follow the standard evolutionary scenario; instead, they evolve onto the super-AGB (e.g., Garcia-Berro & Iben 1994). Initial masses $\geq$11 $M_\odot$ produce final core masses beyond the Chandrasekhar limit and become supernovae. Masses $\gtrsim$50 $M_\odot$ are associated with the luminous blue variables (e.g., Humphreys & Davidson 1994), some of which are in the SWS sample. With all of these sources producing oxygen-rich dust shells, perhaps it is not a surprise that the redder spectra cannot be ordered into a smooth sequence.

Another complication is the mixture of young and old sources in groups 3 and 4 (in contrast to the oxygen-rich spectra in groups 1 and 2 [1.NO and 2.SE], most of which are evolved sources). In subgroup 4.SE, nine of 24 sources are clearly pre–main sequence; all are Herbig Ae/Be stars except for one source classified as F0e. This represents the majority of the young sources in the sample, but three more Herbig Ae/Be stars appear in subgroup 3.SE (out of 21), both 3.SA spectra are pre–main-sequence Be stars, subgroups 4.SEC and 4.SB each contain two pre–main-sequence sources (out of 10 and seven, respectively), and one of the 14 4.SC sources is young (a T Tauri star). Three of the four young sources in subgroups 4.SEC and 4.SB are Herbig Ae/Be stars; the other source is an Ae star.

It is unfortunate that young and old sources appearing in the same part of the H-R diagram, luminous Be, Ae, Fe, and G stars, exhibit similar infrared spectral characteristics. Determining whether these sources were evolving *to* or *from* the main sequence has been a long-standing problem in astronomy. Walker et al. (1989) showed that some types of young and old stars could be separated into different zones using *IRAS* color-color diagrams. As Figures 4 and 5 show, the SWS spectra extend sufficiently beyond 20 μm for the shape of the continuum to be defined, thus showing the underlying dust temperature. The shape of the dust continuum from ~20 to ~40 μm might be one way of separating the young and old objects. Potentially, the more detailed level 3 classification will address this issue.

4.3.3. *The Carbon-Rich Dust Sequence*

While oxygen-rich dust can occur in both evolved stars and environments associated with star formation, carbon-rich dust only occurs in the vicinity of carbon stars or in PNs that have presumably evolved from carbon stars. Furthermore, the range of stellar masses that evolve to carbon stars is limited to $\gtrsim$2 $M_\odot$ and less than several $M_\odot$ (see Wallerstein & Knapp 1998 and references therein). Perhaps for these reasons, the carbon-rich spectral classes defined here fall into a reasonably ordered evolutionary sequence: 1.NC $\rightarrow$ 2.CE $\rightarrow$ 3.CE $\rightarrow$ 3.CR $\rightarrow$ 4.CR $\rightarrow$ 4.CN.

As the mass-loss rate from a naked star with a carbon-rich photosphere (1.NC) grows, its infrared spectrum develops a strong emission feature at ~11.5 μm from SiC, producing a 2.CE spectrum. Further increases in mass-loss rate lead to a cooler, optically thicker shell that enshrouds the central star. The spectrum is then classified as 3.CE. It next evolves to 3.CR as the emitting layer of the dust shell cools and amorphous carbon begins to dominate the spectrum. Further thickening of the dust shell shifts the spectrum to 4.CR. The next stage is less certain because the relation of 4.CT to the sequence is not clear. Perhaps spectra evolve from 4.CR to 4.CN (i.e., to carbon-rich PPNs), and only some unusual circumstances lead to the development of a 4.CT spectrum. Possibly, all carbon-rich sources pass briefly through this stage. However, the latter possibility seems unlikely given the difficulty of fitting the 4.CT spectra into the rest of the carbon sequence.

5. SUMMARY

We examined and categorized the entire *ISO*-SWS database of 1248 SWS01 full-grating spectra. A comprehensive spectral classification system was developed according to the shape of the SED, that is, the temperature of the strongest emitter. Groups were further subdivided based on spectral features such as silicate emission, ice absorption, or fine-structure lines. Most sources that had LRS-based classifications are in similar categories based on their SWS spectra. Where discrepancies occur, e.g., in carbon- versus oxygen-rich or red versus blue SEDs, the SWS classification should take precedence because of the larger bandpass, higher resolution (spectral and angular), and greater sensitivity of SWS. As the level 3 effort progresses, some shifting of individual sources may occur, but the overall classification system should be robust.

K. E. K. would like to thank the National Research Council for support via a Research Associateship through

the Air Force Office of Scientific Research. This work was supported in part by a NASA grant for the analysis of *ISO* dedicated-time observations. S. D. P. acknowledges the efforts of Thijs de Graauw in conducting this experiment. As the SWS Principal Investigator, his advocacy for the STARTYPE and related experiments was critical in obtaining the spectra of sources in the "missing" classes. S. D. P. also thanks Thijs de Graauw, Harm Habing, and Martin Kessler for contributing a portion of their allocated observing time to this experiment. Timo Prusti helped considerably by providing the dedicated- and open-time SWS01 observing lists that allowed us to efficiently retarget the STARTYPE sources. Russ Shipman provided helpful insight into the calibration of the SWS Interactive Analysis software and provided an early version of OLP 10.0. This research has made use of NASA's Astrophysics Data System Abstract Service, SIMBAD, and the on-line Dictionary of Nomenclature of Celestial Objects of the CDS.

APPENDIX A

THE CLASSIFICATIONS

Table 6 contains the group and subgroup classification for each source. Sources are ordered by increasing right ascension. The first and second columns contain the source identification and TDT number of the observation; the observed R.A. and decl. (J2000.0) are given in the third and fourth columns. The classification is in the fifth column, and comments found in the table notes are in the last column. The coordinates are as given by the observer and represent the nominal telescope pointing. They can differ by up to several arcseconds with respect to the nominal coordinates of a given object.

The comments can contain important information regarding the reliability of the spectra and their classifications. The most important two comments are "F" and "W." "F" indicates that a quality flag was attached to the data, either telemetry, pointing, or unknown. Of the 34 flagged observations, 19 could be classified, whereas the rest are in group 7 and are probably irrecoverable. Sources with "W" in the comment column were observed at the wrong coordinates. Two of these were classified based on the detected flux, although a well-centered observation might produce a different classification. Note that an observation does not get a "W" if the observer simply mislabeled the object.

A1. SOURCE NAMES

Given the heterogeneity of the source names in the IDA, not to mention the inaccuracy or nonstandard nature of some names (e.g., GL989 [*sic*] for AFGL 899), the source identification is not necessarily that given by the original observer. Coordinates for each observation were submitted to SIMBAD for a list of all objects within 30″. Although this process is subject to the errors known to be in SIMBAD, it succeeded in identifying most "Off" or "Reference" positions, as well as those sources with incorrect coordinates (e.g., the observer submitted B1950.0 instead of J2000.0 coordinates).

Generally, we preferred older catalog names over newer designations. For example, we used the Greek + constellation designation over a variable star name, HR over HD, and HD over SAO. Similarly, for nebulae, the Messier number takes precedence over NGC or IC names. However, there are exceptions. If a newer name contains useful information, it might be used

TABLE 6
SOURCE CLASSIFICATION

Name	TDT	R.A. (J2000.0)	Decl. (J2000.0)	Group	Comments
W Cet.....	37802225	00 02 07.70	−14 40 35.9	2.SEa:	
SV And	42801007	00 04 20.00	40 06 37.2	2.SEa:	
SV And	80800708	00 04 20.00	40 06 37.2	2.SEa	
CIT 1	78201008	00 06 52.30	43 04 36.0	7	W
HR 10	37802001	00 07 18.20	−17 23 13.2	1.NM:	
β Cas.....	28501420	00 09 10.47	59 08 59.8	1.N	
V633 Cas.....	43501514	00 11 26.60	58 50 04.0	5.SE	W
NGC 40	44401917	00 13 00.91	72 31 20.0	4.PN	
NGC 40	30003803	00 13 01.10	72 31 19.1	4.PN	
HR 48	55502138	00 14 38.40	−18 55 58.4	1.NO	

NOTE.—Units of right ascension are hours, minutes, and seconds, and units of declination are degrees, arcminutes, and arcseconds. Comments include: F = quality flag such as pointing or telemetry problems; G = extragalactic source; W = wrong coordinates; o: = probably an off, but odd in some way; R, R: = possibly a recoverable group 7; H = probably irrecoverable in group 7; Offset = name includes offsets from nominal position indicated by (0, 0); Propn = Name from original observer. M1: (0, 0) position is $(\alpha, \delta) = (05^{h}34^{m}31\overset{s}{.}97,\ 22°00'52\overset{''}{.}1)$ (J2000.0; Han & Tian 1999); M17: (0, 0) position is $(\alpha, \delta) = (18^{h}20^{m}24\overset{s}{.}83,\ -16°11'34\overset{''}{.}9)$ (J2000.0; Johnson, Dupree & Goss 1998); Cas A: (0, 0) position is the Chandra point source $(\alpha, \delta) = (23^{h}23^{m}27\overset{s}{.}94,\ 58°48'42\overset{''}{.}4)$ (J2000.0; Tananbaum 1999).Table 6 is published in its entirety in the electronic edition of the *Astrophysical Journal Supplement*. A portion is shown here for guidance regarding its form and content.

instead of an older one. For instance, WR (Wolf-Rayet stars) and MWC (emission-line stars) numbers are used instead of HD numbers as appropriate. Another exception to the age preference are Flamsteed numbers, which were generally avoided unless the source is commonly referenced in the literature by that name (five sources). When in doubt as to what to call a source, we tried to follow the most common usage in the literature as a guide.

A number of observations have no apparent counterpart in the SIMBAD database. In these cases (37), the names given by the observer are used, and their origin is indicated by a notation (" Propn ") in the comment column of the table. Objects in the Galactic center have " GC " attached to their designations. An example of both these situations is GC SE_NTF_Xng, where the observer called this position SE_NTF_Xng, presumably a nonthermal filament crossing in the southeast; adding the " GC " indicates that it is a Galactic center object.

There are also observations of the same source at different positions. These objects were typically either calibration sources, such as γ Dra and α Boo, or extended objects, such as Cas A or M17. A nominal (0, 0) position was chosen for each source. The offsets for a particular observation are then included in the name. For example, α Boo -0.39, $+3.4$ is $(\Delta\alpha, \Delta\delta) = (-0^{s}.39,\ 3''.4)$ from α Boo. A total of 19 objects and 91 observations have this type of name and are noted with " Offset " in the comment column.

REFERENCES

Aoki, W., Tsuji, T., & Ohnaka, K. 1998, A&A, 333, L19
———. 1999, A&A, 350, 945
Begemann, B., Dorschner, J., Henning, T., Mutschke, H., & Thamm, E. 1994, ApJ, 423, L71
Cannon, A. J., & Pickering, E. C. 1918, Ann Astron. Obs. Harvard Coll., 91, 1
Cernicharo, J., Yamamura, I., González-Alfonso, E., de Jong, T., Heras, A., Escribano, R., & Ortigoso, J. 1999, ApJ, 526, L41
Cheeseman, P., Stutz, J., Self, M., Taylor, W., Goebel, J., Volk, K., & Walker, H. 1989, Automatic Classification of Spectra from the Infrared Astronomical Satellite (NASA RP-1217; Washington, DC: GPO)
Cohen, M., Walker, R., Wainscoat, R., Volk, K., Walker, H, & Schwartz, D. 1990, An Infrared Sky Model Based on the *IRAS* Point Source Data (NASA-CR-177526) (Washington, DC: NASA)
Creech-Eakman, M. J., Stencel, R. E., Williams, W. J., & Klebe, D. I. 1997, ApJ, 477, 825
de Graauw, T., et al. 1996, A&A, 315, L49
Egan, M. P., & Sloan, G. C. 2001, ApJ, 558, 165
Engelke, C. W. 1992, AJ, 104, 1248
Fouks, B. I. 2001, in The Calibration Legacy of *ISO*, ed. L. Metcalfe & M. F. Kessler (SP-481; Noordwijk: ESA), in press
Fouks, B. I., & Schubert, J. 1995, Proc. SPIE, 2475, 487
Garcia-Berro, E., & Iben, I. 1994, ApJ, 434, 306
Goebel, J. H., Bregman, J. D., Strecker, D. W., Witteborn, F. C., & Erickson, E. F. 1978, ApJ, 222, L129
Goebel, J. H., et al. 1980, ApJ, 235, 104
Goebel, J. H., & Moseley, S. H. 1985, ApJ, 290, L35
Goebel, J., Volk, K., Walker, H., Gerbault, F., Cheeseman, P., Self, M., Stutz, J., & Taylor, W. 1989, A&A, 222, L5
Han, J. L., & Tian, W. W. 1999, A&AS, 136, 571
Hearnshaw, J. B. 1986, The Analysis of Starlight: One Hundred and Fifty Years of Astronomical Spectroscopy (Cambridge: Cambridge Univ. Press)
Hony, S., et al. 2000, A&A, 355, 187
Hron, H., Loidl, R., Jørgensen, U. G., Aringer, B., & Kerschbaum, F. 1998, A&A, 335, L69
Humphreys, R. M., & Davidson, K. 1994, PASP, 106, 1025
IRAS Explanatory Supplement 1988, Catalogs & Atlases, Vol. I (Washington, DC: NASA)
IRAS Science Team 1986, A&AS, 65, 607
Johnson, C. O., Dupree, C. G., & Goss, W. M. 1998, ApJ, 500, 302
Jones, T. J., Bryja, C. O., Gehrz, R. D., Harrison, T. E., Johnson, J. J., Klebe, D. I., & Lawrence, G. F. 1990, ApJS, 74, 785
Jørgensen, U. G., Hron, J., & Loidl, R. 2000, A&A, 356, 253
Justtanont, K., Feuchtgruber, H., de Jong, T., Cami, J., Waters, L. B. F. M., Yamamura, I., & Onaka, T. 1998, A&A, 330, L17
Kessler, M. F., et al. 1996, A&A, 315, L27
Kester, D., Fouks, B., & Lahuis, F. 2001, in The Calibration Legacy of *ISO*, ed. L. Metcalfe & M. F. Kessler (SP-481; Noordwijk: ESA), in press
Kraemer, K. E., Sloan, G. C., & Price, S. D. 2001, in The Calibration Legacy of *ISO*, ed. L. Metcalfe & M. F. Kessler (SP-481; Noordwijk: ESA), in press
Kwok, S., Volk, K., & Bidelman, W. P. 1997, ApJS, 112, 557
Lamers, H. J. G. L. M., et al. 1996, A&A, 315, L229
Leech, K. J., et al. 2001, The *ISO* Handbook, Vol. VI: SWS—the Short Wavelength Spectrometer
Little-Marenin, I. R. 1986, ApJ, 307, L15
Little-Marenin, I. R., & Little, S. J. 1988, ApJ, 333, 305
———. 1990, AJ, 99, 1173
Little-Marenin, I. R., & Price, S. D. 1986, in Summer School on Interstellar Processes, ed. D. J. Hollenbach & H. A. Thronson (NASA Technical Memorandum 88342; Moffet Field: NASA/ARC), 137
Little-Marenin, I. R., Ramsey, M. E., Stephenson, C. B., Little, S. J., & Price, S. D. 1987, AJ, 93, 663
Lloyd Evans, T. 1990, MNRAS, 243, 336
Lorenz-Martins, S., & Pompeia, L. 2000, MNRAS, 315, 856
Martin, P. G., & Rogers, C. 1987, ApJ, 322, 374
Molster, F. J., Yamamura, I., Waters, L. B. F. M., Nyman, L.-Å., Käufl, H.-U., de Jong, T., & Loup, C. 2001, A&A, 366, 923
Monnier, J. D., Geballe, T. R., & Danchi, W. C. 1998, ApJ, 502, 833
Morgan, W. W. 1938, ApJ, 87, 460
Morgan, W. W., Keenan, P. C., & Kellman, E. 1943, An Atlas of Stellar Spectra, with an Outline of Spectral Classification (Chicago: Univ. Chicago Press)
Morris, P. W., van der Hucht, K. A., Crowther, P. A., Hillier, D. J., Dessart, L., Williams, P. M., & Willis, A. J. 2000, A&A, 353, 624
Onaka, T., de Jong, T., & Willems, F. J. 1989, A&A, 218, 169
Pickering, E. C. 1890, Ann. Astron. Obs. Harvard Coll., 17, 1
Price, S. D., & Murdock, T. L. 1983, The Revised AFGL Infrared Sky Survey Catalog, Document AFGL-TR-83-0161, Air Force Geophysics Laboratory
Rutherford, L. M. 1863, Am. J. Sci. Arts, 35, 71
Secchi, A. 1866, Comptes Rendus, 63, 364
———. 1868, Comptes Rendus, 67, 373
Shipman, R. F., et al. 2001, in The Calibration Legacy of *ISO*, ed. L. Metcalfe & M. F. Kessler, (SP-481; Noordwijk: ESA), in press
Sloan, G. C., & Egan, M. P. 1995, ApJ, 444, 452
Sloan, G. C., Goebel, J. H., Kraemer, K. E., & Price, S. D. 2001a, BAAS, 199, 92.04
Sloan, G. C., Kraemer, K. E., & Price, S. D. 2001b, in The Calibration Legacy of *ISO*, ed. L. Metcalfe & M. F. Kessler (ESA: SP-481; Noordwijk: ESA), in press
Sloan, G. C., & Price, S. D. 1995, ApJ, 451, 758
———. 1998, ApJS, 119, 141
Sylvester, R. J., Kemper, F., Barlow, M. J., de Jong, T., Waters, L. B. F. M., Tielens, A. G. G. M., & Omont, A. 1999, A&A, 352, 587
Tananbaum, H. 1999, IAU Circ., 7246, 1
van Winckel, H., Waelkens, C., & Waters, L. B. F. M. 1995, A&A, 293, L25
Vogel, H. C. 1874, Astron. Nachr., 84, 113
Vogel, H. C., & Wilsing, J. 1899, Publ. Astrophys. Obs. Potsdam, 12, 1
Volk, K., Kwok, S., Stencel, R. E., & Brugel, E. 1991, ApJS, 77, 607
Volk, K., Xiong, G.-Z., & Kwok, S. 2000, ApJ, 530, 408
Wainscoat, R. J., Cohen, M., Volk, K., Walker, H. J., & Schwartz, D. E. 1992, ApJS, 83, 111
Walker, H. J., & Cohen, M. 1988, AJ, 95, 1801
Walker, H. J., Cohen, M., Volk, K., Wainscoat, R. J., & Schwartz, D. E. 1989, AJ, 98, 2163
Wallerstein, G., & Knapp, G. R. 1998, ARA&A, 36, 369
Waters, L. B. F. M., et al. 1996, A&A, 315, L361
Yamamura, I., Dominik, C., de Jong, T., Waters, L. B. F. M., & Molster, F. J. 2000, A&A, 363, 629